




REVIEW ARTICLE

Chemical modification of ordered/disordered carbon nanostructures for metal hosts and electrocatalysts of lithium-air batteries

Jeongyeon Lee^{1,2}  | Tae Hyung Lee³ | Ho Won Jang³  | Ho Seok Park¹ 

¹School of Chemical Engineering, Convergence Research Center for Energy and Environmental Sciences, Department of Health Sciences and Technology, Samsung Advanced Institute for Health Sciences and Technology (SAIHST), Sungkyunkwan University (SKKU), Suwon, Republic of Korea

²Institute of Textiles Clothing, The Hong Kong Polytechnic University, Hung Hom, Hong Kong SAR, China

³Department of Materials Science and Engineering, Research Institute of Advanced Materials, Seoul National University, Seoul, Republic of Korea

Correspondence

Ho Won Jang, Department of Materials Science and Engineering, Research Institute of Advanced Materials, Seoul National University, Seoul 08826, Republic of Korea.

Email: hwjang@snu.ac.kr

Ho Seok Park, School of Chemical Engineering, Convergence Research Center for Energy and Environmental Sciences, Department of Health Sciences and Technology, Samsung Advanced Institute for Health Sciences and Technology (SAIHST), Sungkyunkwan University (SKKU), 2066 Seobu-ro, Jangan-gu, Suwon 16419, Republic of Korea.

Email: phs0727@skku.edu

Funding information

National Research Foundation of Korea, Grant/Award Numbers:

2020M2D8A206983011, NRF-

2020M2D8A2070866,

2020M3H1A1077095; Basic Science

Research Program funded by the Ministry of Science, ICT & Future Planning, Grant/Award Number: 2021R1A2B5B03001851

Abstract

Although lithium-air batteries (LABs) are considered the promising alternative of existing lithium-ion batteries owing to their high energy density of 11 680 W h kg⁻¹, their practical applications are limited by the technical issues, such as unstable solid electrolyte interface and dendrite formation from metal anode and insufficient bifunctional activities and durability from cathode catalyst. In order to resolve these bottlenecks, carbon nanostructures have been investigated owing to their high surface area, excellent electrical conductivity, electrochemical stability, and various modification chemistries. Herein, we comprehensively review a recent progress on the design of carbon nanostructures for their applications into metal hosts, protection layers, and bifunctional electrocatalysts of LABs. The correlation between the crystalline, electronic, porous, and chemical structures and the electrochemical properties of carbon nanomaterials are discussed depending on their classification and characteristics. Various chemical modifications, such as morphological control, hierarchical architecturing, heteroatom incorporation, and the formation of composites, for the improved electrochemical performances of anode and cathode will be also addressed. Furthermore, we deal with the perspectives for the ongoing obstruction and future guidance.

KEYWORDS

bifunctional catalysts, carbon nanostructures, lithium-air batteries, metal anodes, surface modification

This is an open access article under the terms of the Creative Commons Attribution License, which permits use, distribution and reproduction in any medium, provided the original work is properly cited.

© 2021 The Authors. *InfoMat* published by UESTC and John Wiley & Sons Australia, Ltd.

1 | INTRODUCTION

Over the several decades, the consumption of fossils fuels and electricity has rapidly increased as the consequence of the development of the modern society and industry.^{1–4} The massive demand of energy causes diverse environmental problems including the global warming, the atmosphere pollution by the release of greenhouse and pollution gases, such as CO₂, SO₂, and NO_x gases, and the particulate matter. In addition to these problems, the emerging markets such as future portable electronics and electric vehicles push forward the development of advanced energy storage devices with the high energy density and safety.^{5,6} As a champion technology, the rechargeable lithium-ion battery (LIB) has drawn tremendous interest from both academics and industry owing to it higher energy density than those of other commercial batteries.^{7,8} However, LIBs cannot satisfy increasing demands and requirements for the high performance, safety, and low cost. Thus, next-generation rechargeable batteries have been developed to resolve these issues for emerging applications and renewable energy storage.^{9–12}

Among various next-generation energy storage devices, metal-air batteries (MABs) are considered the promising alternative to existing LIBs owing to their high energy density (e.g., 3500 W h kg^{−1} for Li-air batteries).^{13–15} MABs consist of a metal anode, an “oxygen/air” cathode, which occurs the typical electrocatalytic reactions, such as oxygen reduction reaction (ORR) and oxygen evolution reaction (OER), and electrolytes.¹⁶ When the charging/discharging process is totally reversible with the infinite amount of oxygen source and metal anode is recovered via recharging process, MABs can be operated in a continuous manner.^{17,18} Therefore, the MAB system has a potential as new generation batteries to be truly competitive to typical Li-ion batteries and has been extensively investigated covering Li-,¹⁹ Na-,^{20,21} Zn-,²² Al-,^{23,24} Fe-,²⁵ and Mg-air batteries.²⁶ However, MABs still have fundamental and technical issues for real applications. Firstly, major problems associated with the anode side are the excessive growth of metal dendrites and the uneven solid electrolyte interphase (SEI) formation from the surface of metal anodes.^{27,28} Especially, Li-metal anode, the commonly used anode for Li-air battery (LAB), can deteriorate the performance and safety of the battery cells due to the unstable SEI formation and dendrite growth on the surface of the metal anode.²⁹ Various chemical approaches using carbonaceous materials as the protection layer and metal hosts have been developed to circumvent these problems for high performance and safe LABs. For example, Luo et al. investigated the enhanced performance of Li-O₂ batteries with the

reduced graphene oxide (rGO)/Li anode, where rGO suppressed the Li dendrite and unstable SEI layer resulting in stable battery performance.^{30,31}

The operation of LABs also relies on the design of cathode material with bifunctional electrocatalysts. Thus, it is needed to develop the efficient and robust bifunctional catalysts for achieving the high rechargeability of LABs and the reduced voltage hysteresis during cyclic performances, resulting in the advanced LAB performances with high energy efficiency and stable long-term cyclability.³² Since the charging and discharging processes of LABs are associated with OER and ORR, respectively, on the cathode, the advanced electrocatalysts of a cathode are imperative to lower the overpotential required for those redox reactions and to promote facile and reversible charging/discharging process.³³ In particular, the highly active bifunctional catalysts are important for achieving rechargeability and reversibility of LABs because both OER and ORR occur at the same electrode.³⁴ Among bi- or multifunctional electrocatalysts, noble metals as Pt, Ru, Ir, and their oxides have been widely used as excellent electrocatalysts. However, their high costs from their rarity and insufficient long-term durability limit the practical applications of LABs. Moreover, Ru and Ir oxides are weak in ORR, while Pt is unfavorable in OER.³⁵ Various active and stable bifunctional electrocatalysts, including transition metals, metal oxides, sulfides and their composites, have been extensively investigated to overcome these bottlenecks.^{36–38} However, metal-based catalysts still have some disadvantages, such as relatively high cost, scarcity, and poor long-term cyclability.³⁹ The metal-free or metal-less nanostructured carbon electrocatalysts have drawn special attention owing to their versatile functionality, earth abundance, low cost, and durability. As the pioneering work of metal-free carbon materials for ORR, Dai et al. reported vertically aligned nitrogen-doped carbon nanotubes with significantly improved long-term operational stability, electrocatalytic activities, and stability.⁴⁰ Then, diverse carbon compounds, such as carbon nanotubes, graphene, graphite, and porous carbon with heteroatom doping, structural control, or polymer composite, have been exploited to achieve high catalytic activities for ORR and OER.⁴¹

In this article, we aim at critically and comprehensively reviewing the fundamental understanding about the structure and properties of carbon materials, as well as their applications into metal hosts, protection layers, and electrocatalysts of LABs. More specifically, this review focuses on the classification and characteristics of various carbon materials for their chemical structure, crystallinity, and porosity, as well as the modification process of carbon materials including morphology design,

surface functionalization, and metal-free composite. Furthermore, we deal with the correlation between structure and property of carbon materials in LABs and the perspectives for the ongoing obstruction and future guidance.

2 | STRUCTURES AND MODIFICATIONS OF NANOSTRUCTURED CARBON MATERIALS

2.1 | Types of carbonaceous materials

As shown in Figure 1, various factors, such as the types of precursors, reaction temperature, and materials' phases, are considered for the synthesis of carbonaceous materials, determining the degree of the orderness of carbonaceous materials. Depending on the degree of orderness, carbonaceous materials can be categorized into graphite, hard carbon, and soft carbon.⁴² Firstly, an ordered three-dimensional (3D) sp^2 hybridized carbon, or graphite, is composed of the stacked graphene layers along the c-axis. As lower dimensional carbon allotropes, the graphene is a honeycomb like 2D structure of sp^2 hybridized ordered carbon with high crystallinity.^{43,44} In addition, 1D carbon nanotubes (CNTs) are regarded as seamless cylinder type of graphene.⁴⁵ On the other hand, hard and soft carbon can be classified into the disordered carbon materials. The disordered soft carbon can be converted into ordered structure such as graphite via the

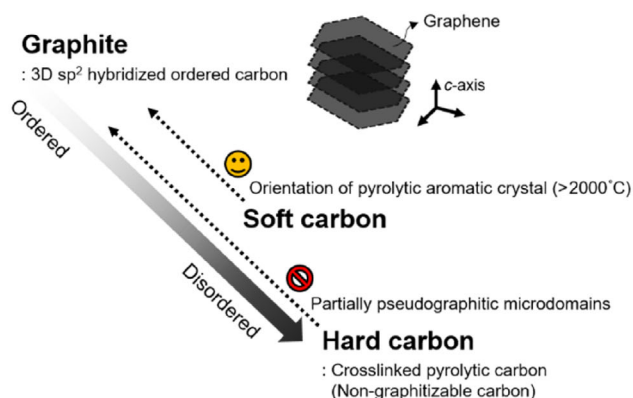
heat treatment at high temperatures (over 2000°C), which leads to well-oriented graphitized aromatic crystals. On contrary, hard carbons are non-graphitizable, because their cross-linked pyrolytic structure prevents the graphitization even at extremely high temperatures (>3000°C). Therefore, hard carbons with turbostratic structure have a short-range orderness due to the irregular distribution of pseudo-graphitic microdomains.

2.2 | Design of nanostructured carbonaceous materials

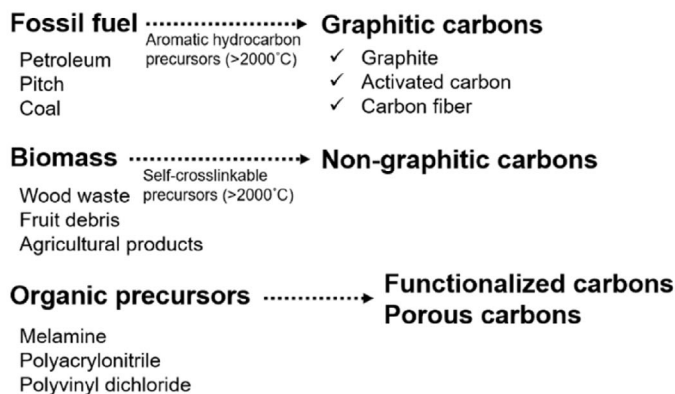
2.2.1 | Raw materials for carbonaceous materials

Carbon materials can be synthesized by the calcination of fossil fuel, biomass, and other organic precursors in inert gas. As shown in Figure 1, representative carbon materials, such as graphite, activated carbon, and carbon fiber, are derived from the fossil fuels, such as petroleum and coal. Since the excessive use of fossil fuel causes the severe environment issues, such as global warming and climate change, carbon materials have been synthesized using more renewable biomass, such as wood waste, fruit debris, and agricultural products.⁴⁶ Another approach for the design of functionalized or porous carbon materials is to use the carbon-rich organic precursors (polymers), such as melamine, polyacrylonitrile (PAN), and polyvinyl dichloride. According to the chemical compositions of organic precursors, various heteroatom-doped carbon

(1) Types of carbonaceous materials



(2) Raw materials for carbonaceous materials



(3) Catalytic graphitization for high crystalline carbonaceous materials

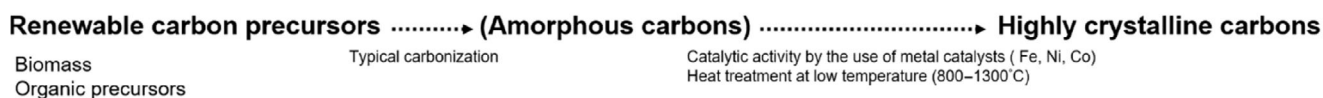


FIGURE 1 Schematic illustrations of the types of carbon materials and the carbon precursors

materials can be obtained. In particular, the nature of precursors (i.e., fossil fuel, biomass, and polymer) can affect the crystallinity of carbon materials. Biomass and organic precursors with high oxygen content and impurity can be transformed to non-graphitic carbons after calcination owing to their self-crosslinking reaction at a low temperature, which prevents well-stacked ordering. The intrinsic properties of precursors for fossil fuel and biomass can determine the graphitization degree of carbon materials (soft or hard carbon), depending on biomass with cross-linkable precursors or fossil fuels with aromatic hydrocarbon structure at a high temperature ($>2000^{\circ}\text{C}$). Normally, the graphite is derived from pitch or petroleum coke, nonrenewable carbon sources at high temperatures (2000 to 3500°C), which takes few weeks to convert amorphous carbon into graphite with high crystallinity.⁴⁷ This graphitization process also requires huge energy and production cost, as well as environment issues by the use of nonrenewable carbon precursors. Accordingly, the simple graphitization process with renewable carbon precursors at comparably low temperatures is needed to synthesize graphitic carbons. Catalytic graphitization is an effective approach to transform renewable carbon precursors into highly crystalline carbon materials at low temperatures (800 to 1300°C). This strategy requires some metal catalysts, such as iron (Fe), nickel (Ni), and cobalt (Co) to convert amorphous carbons into graphitic carbon materials by their catalytic activity of metals.^{48–50} For example, Schnepf et al. reported the transformation of lignocellulosic biomass into nanostructured graphitic carbon by catalytic iron carbide nanoparticles, which generate the intertwined graphitic tubules during the catalytic thermal decomposition at 800°C .⁵¹

2.2.2 | Synthesis methods of various carbonaceous materials

Top-down techniques, such as mechanical cleavage,⁵² electrochemical exfoliation,⁵³ and liquid-phase exfoliation (LPE),⁵⁴ are generally utilized for obtaining few-layered nanosheets or nanocomposites from various bulk materials. As a feasible approach to fabricate the individual nanosheets, mechanical exfoliation endorses mechanical forces to physically disrupt the weak van der Waals interactions between layers of bulk materials. Novoselov et al. first explored a monolayer graphene by the exfoliation in 2004, where the adhesive tape was used to peel off the carbon flakes from graphite.⁵⁵ Since this pioneer work, various mechanical exfoliation methods have been studied. For example, Sutter and coworkers used a few-layered graphene by using the modified mechanical

exfoliation method to obtain the thin graphene flakes with high yield and large area as shown in Figure 2A.⁵⁶ The simple annealing stage of the substrate was applied to increase contact area with graphite by the adhesive tape, and the resulting graphene flakes were 20–60 times larger than those of previous ones.

Among the typical mechanical exfoliation approaches, the electrochemical exfoliation techniques that adopt the intercalation of charged electrolyte species into layers by the positive and negative voltage differences have been applied to isolate single or few layers from bulk materials.⁶² As shown in Figure 2B, Su et al. obtained the bilayered graphene with A-B stacking with lateral size of $\sim 30\text{ }\mu\text{m}$ through one-step electrochemical exfoliation method in sulfuric acid.⁵⁷ Sonication-assisted LPE is commonly used to extract individual layers from bulk materials in liquid environments. This process is followed by three steps: (1) dispersion of bulk materials in a solvent, (2) LPE, and (3) filtration. Under the ultrasonication process, the vigorous bubbles are generated by vibration waves, which create the strong tensile stress exerted to the layered materials to boost the exfoliation.⁶³ This LPE method without surfactants or intercalants is facile and cost-effective, but the method gives extremely low yield. Therefore, the post-LPE approaches, like intercalant-assisted LPE, have been employed with selected ions or organic molecules as intercalants. These intercalants can be inserted between layers of bulk materials to compose the ion/molecule species of intercalated compounds so that noncovalent π – π interaction of layers is weakened and interspacing is expanded.⁶⁴ In Figure 2C, Stoddart et al. reported the direct exfoliation method of graphene using N,N'-dimethyl-2,9-diazaperopyrenium dication (MP^{2+}) molecules as intercalants in both organic solvents and water. The as-prepared graphene sheets could be well dispersed in water, which shows the excellent dispersion stability for few weeks.⁵⁸

Bottom-up methods involve the synthesis techniques of few-layered structures directly from small molecules or ions. The chemical vapor deposition (CVD) method is a typical bottom-up approach to directly grow 2D nanosheet. In CVD process, the preferred carbon sources, such as methane, acetylene, xylene, and ethanol, and typical metal substrates, such as Si, SiO_2 , Ni, and Cu, are commonly used.^{65–68} Various carbon sources react on metal substrates at the high temperature, which lead to atomic deposition and growth mechanism on substrates. As shown in Figure 2D, Ann et al. successfully demonstrated the growth mechanism of graphene films on wafer-scale Ni or Cu substrate, as followed by direct etching of metal layers and transfer methods for the fabrication of wafer-sized and high-quality graphene films.⁵⁹ Accordingly, mono-/bi-layered graphene grown on the

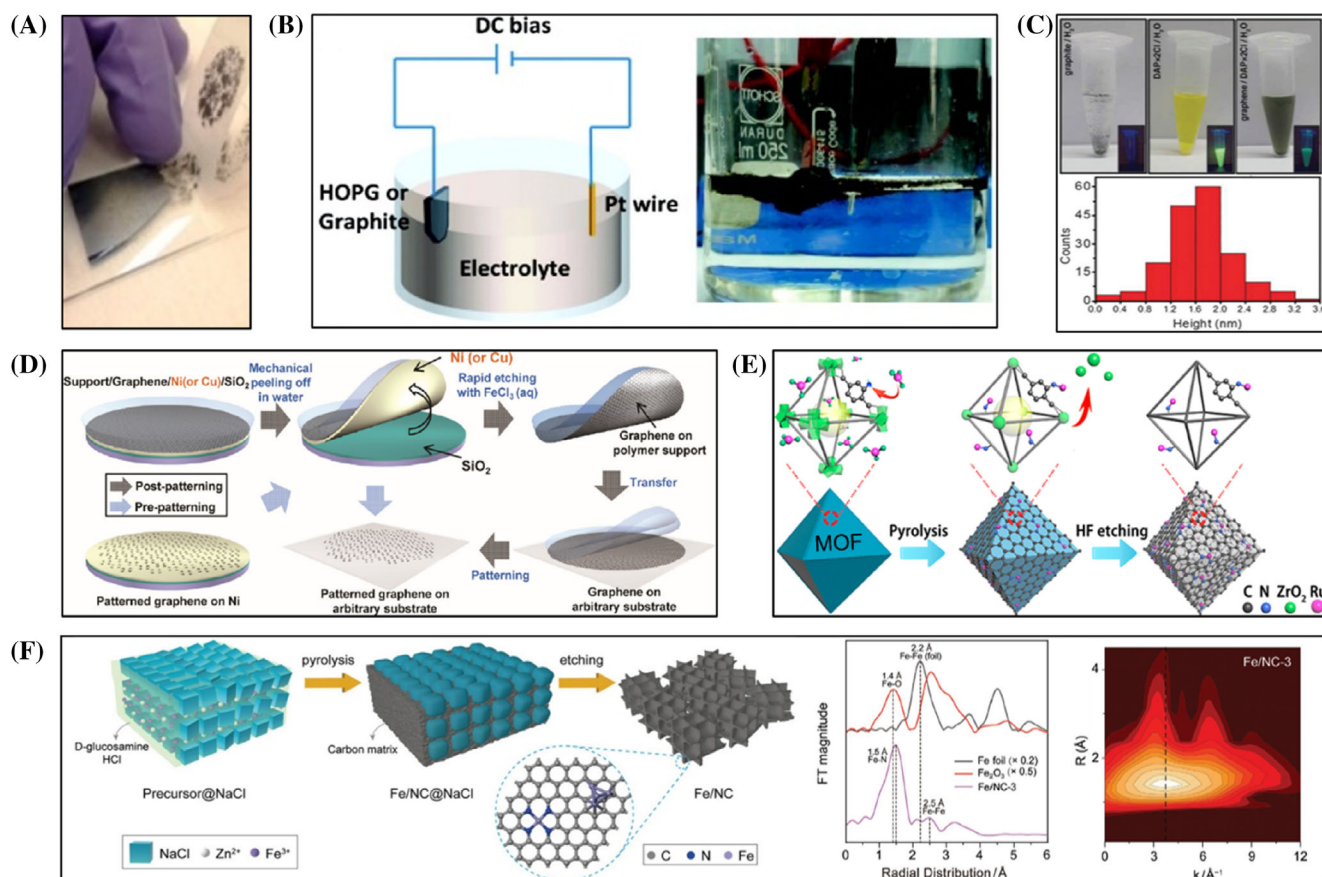


FIGURE 2 (A) Illustrations of the modified exfoliation process of graphene.⁵⁶ Reproduced with permission, 2015, American Chemical Society. (B) Illustration and photo for electrochemical exfoliation of graphite.⁵⁷ Reproduced with permission, 2011, American Chemical Society. (C) the preparation of graphene by an organic solvent-based exfoliation and calculation of the thickness of the graphene sheets by atomic force microscopy.⁵⁸ Reproduced with permission, 2015, Wiley-VCH. (D) Illustrations of the synthesis, etching, and transfer of large-area graphene films by a chemical vapor deposition method.⁵⁹ Reproduced with permission, 2010, American Chemical Society. (E) Scheme of formation process of Ru SAs/N-doped carbon.⁶⁰ Reproduced with permission, 2017, American Chemical Society. (F) Schematic illustration of the synthetic mechanisms for Fe SAs embedded in N-doped carbon, and FT profiles of Fe K-edge k^2 -weighted EXAFS data and wavelet transforms for EXAFS signals.⁶¹ Reproduced with permission, 2021, Wiley-VCH

substrate was directly synthesized, achieving the high conductivity and transparency, as well as the flexibility for the practical applications, such as solar cells and flexible devices. These reports exemplify the potential of those graphene materials and bottom-up approach to prepare high purity graphene. However, further researches are still required to realize the mass-production of high-quality graphene mono- or bi-layers.

There are various synthesis methods of nanostructured carbon materials, such as hydrothermal/solvothermal methods, hard templating methods, and the carbonization process from carbon precursors (e.g., biomass, organic precursors and metal-organic frameworks).⁶⁹ The hydrothermal/solvothermal synthesis is a facile and scalable way to synthesize the various carbon materials with tailored nanostructure and functionality. Antonietti et al. reported the synthesis of mesoporous carbon materials by the

hydrothermal method with a hard template of silica.⁷⁰ Moreover, the hard templating approach is regarded as the powerful process for producing porous carbonaceous materials. In the hard templating process, the typical inorganic materials, such as silica, NaCl, and metal oxides, are utilized as sacrificial hard templates and removed using the acid or strong base after the formation of carbonization. Nazar et al. prepared the spherical ordered mesoporous carbon nanoparticles with multiple nanopores via the hard templating approach with polymer precursors and spherical silica.⁷¹ On the other hand, the carbonization process of various carbon precursors by the heat treatment has been employed to synthesize the nanostructured carbon materials. According to the component of carbon precursors and types of templates, the various carbon materials with diverse morphology and functionality can be tuned.

2.2.3 | Modification for carbonaceous materials

The nanostructured carbon materials can be modified through the surface functionalization with heteroatoms after carbonization.^{72,73} Compared to nonpolar C—C bonding, the modified carbon materials can form more polar bonding with heteroatoms, which results in achieving different densities of states and charge population for the modified electronic structure and property.^{74,75} For example, nitrogen-doped carbon materials have the distinctively chemical states of nitrogen atom on carbon lattice and edge such as pyridinic, pyrrolic, and graphitic N states, which show different electrocatalytic activities and charge storage properties.⁷⁶ Various co- and tri-doping processes have been studied for improving the electrochemical properties with their synergistic effects of multi-doping. Furthermore, single atom (SA)-embedded carbon materials are attractive as promising catalysts owing to their atomically active sites for good catalytic properties with the stability in the full pH range. Among various metal sites, “M—N—C” sites (M=Fe, Co, Ni, etc.) in SAs/carbon composites derived from the calcination of M—N₄-coordinated macrocycles showed theoretically and experimentally excellent catalytic properties.^{77,78} In Figure 2E, Li et al. reported the synthesis of ruthenium (Ru) SA-embedded nitrogen-doped porous carbon host derived from metal-organic frameworks (MOFs), which is UiO-66-containing zirconium, used as carbon precursors.⁶⁰ Ru SA-embedded nitrogen-doped carbon by employing uncoordinated amine groups on MOFs can provide the atomically isolated dispersion of Ru SA on carbon structure and synergistic effect with Ru sites for electrocatalytic properties. Lee et al. also synthesized an iron (Fe) SA-loaded N-doped carbon matrix by the carbonization process with Fe salts and glucosamines as SA and doping sources, respectively, as well as sodium chloride as hard templates in Figure 2F.⁶¹ These Fe SA/carbon composites revealed the atomically isolated Fe—N—C sites on carbon matrix, which deliver the excellent catalytic activities in universal pH range.

2.3 | Structure and property correlation of carbon materials for metal hosts, protection layers, and electrocatalysts

Despite the advantages of LABs, such as high energy density and abundant oxygen sources, there are still some challenges for practical applications. As shown in Figure 3, the correlation of structure and properties for various carbon materials is summarized. On the anode side, the use of metallic Li causes severe dendrite growth, uneven SEI

layer, volume expansion, and corrosion arising from the accumulation of by-product during the cyclic process. To effectively raise these improvement factors, various carbonaceous materials as metal host and protection layer have been developed for advanced LABs with high performance and cycle stability. On the cathode side, metal-free or -less carbon-based catalysts have been developed to replace the noble and transition metal-based electrocatalysts. In spite of reasonable catalytic activity of noble and transition metals, they are easily oxidized under air atmosphere and limited by unmanageable agglomeration/dissolution in strong universal electrolytes, incurring the unstable long-term cyclability.⁷⁹ To tackle some issues from cathode sides, some improvement factors, such as low active sites and deactivation of catalysts during the long-term cycling, are considered and the structure and properties of nanostructured carbon materials and their modification process are fundamentally understood. Various nanostructured carbon materials with the distinct morphology, such as sphere, tube, fiber, and sheet, have been widely developed and applied for various energy-related applications, owing to their high surface area, excellent electronic conductivity, and strong durability in universal media.⁸⁰ Along with the morphology control of carbon materials, electrocatalytic performances in LABs depend on their degree of orderliness and porous structure, which can affect structural stability, electrical conductivity, and the ion transport. Depending on the pore size, the porous structures of carbon materials can be categorized as macropores, mesopores, and micropores. The macropores and mesopore contribute to provide the fast channel of ions, mitigate the volume expansion for metal anodes, and offer easy access to abundant active sites.⁸¹ On the other hand, micropores, which are generated from physical and chemical activation process of carbon materials, lead to the large surface area and rich active sites.^{82,83}

The structural control of various nanostructured carbon materials, such as porous structure and hierarchical architecture, has been explored to suppress the growth of Li dendrites and to form the stable SEI layer for the effective metal hosts or protection layers of LAB anodes. In addition, the chemical modifications of carbon materials by surface modification, like heteroatom incorporation, defect engineering, and functional group, are exploited to improve the electrochemical performance and stability of LAB cathodes. In sharp contrast to highly graphitic carbon materials with nonpolar property, the polar bonding of carbon materials with heteroatoms can increase the active sites of electrocatalysts. Furthermore, compositional control, such as carbon hybrid, metal-free carbon composites with various conducting polymers, and SAs can facilitate reaction kinetics during OER and ORR, resulting in enhancing the efficiency and lowering the

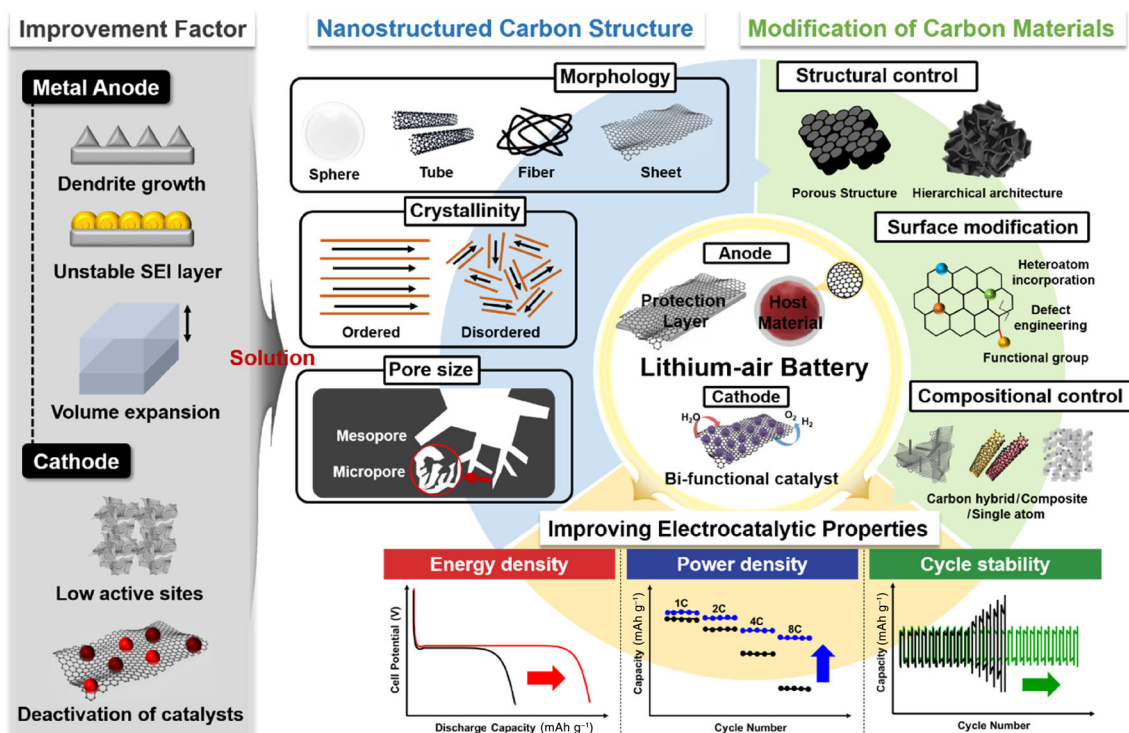


FIGURE 3 Schematic illustrations of structure and property correlation of carbon materials for metal hosts, protection layers, and electrocatalysts in LABs

overpotential during the catalytic reaction. In the following sections, detailed examples of these modifications are discussed.

3 | NANOSTRUCTURED CARBONACEOUS MATERIALS FOR METAL ANODE

Nanostructured carbon materials with bespoke structure have emerged as metal hosts for LABs, owing to their high electrical conductivity, large surface area, electrochemical stability, and chemical modifications. Recently, the template methods for designing the porous carbon materials with various morphology have been widely utilized.^{84–87} For example, Hyeon et al. prepared the carbon structure with bimodal pores by using silica templates, typically used as hard templates, due to their facile removal after carbonization by a base treatment and structural durability.^{84,85} These carbon materials as hosts and protection layers are employed to conduct metal plating and stripping, which can reduce the volume expansion of metal and local current density during the cycling. As mentioned, the carbon materials can be largely classified as graphitic and amorphous carbon structures, depending on the degree of orderness. The surface modification process with heteroatom doping and

nanopores can also convert graphitic carbons, such as graphene and CNT, into functionalized carbon materials with defects. The functionalized carbon materials play a role in providing the favorable metal sites, which assist metal plating onto carbon hosts.⁸⁶ However, excessive defects on carbon materials are risky to reduce the electrical conductivity and to catalyze the electrolyte reduction, resulting in the formation of unstable SEI layer.⁸⁷ Therefore, it is important to understanding the structure and properties of carbon materials and further to optimize the types of carbon and suitable modification process for developing effective Li metal hosts in LABs.

3.1 | Graphitic carbon nanomaterials with functionalization

As a representative ordered carbon material, 2D graphene has advantage in terms of the excellent electrical conductivity, mechanical flexibility, and large surface area. Especially, the chemically modified graphitic carbon materials can suppress the metal dendrite growth and the unstable SEI formation. Lin et al. firstly proposed a melting strategy to synthesize a layered Li-reduced graphene oxide (rGO) composite anode via molten Li infusion into the rGO film with uniform interlayer as shown in Figure 4A.⁸⁸ When graphene oxide (GO) films contacted with molten Li, a

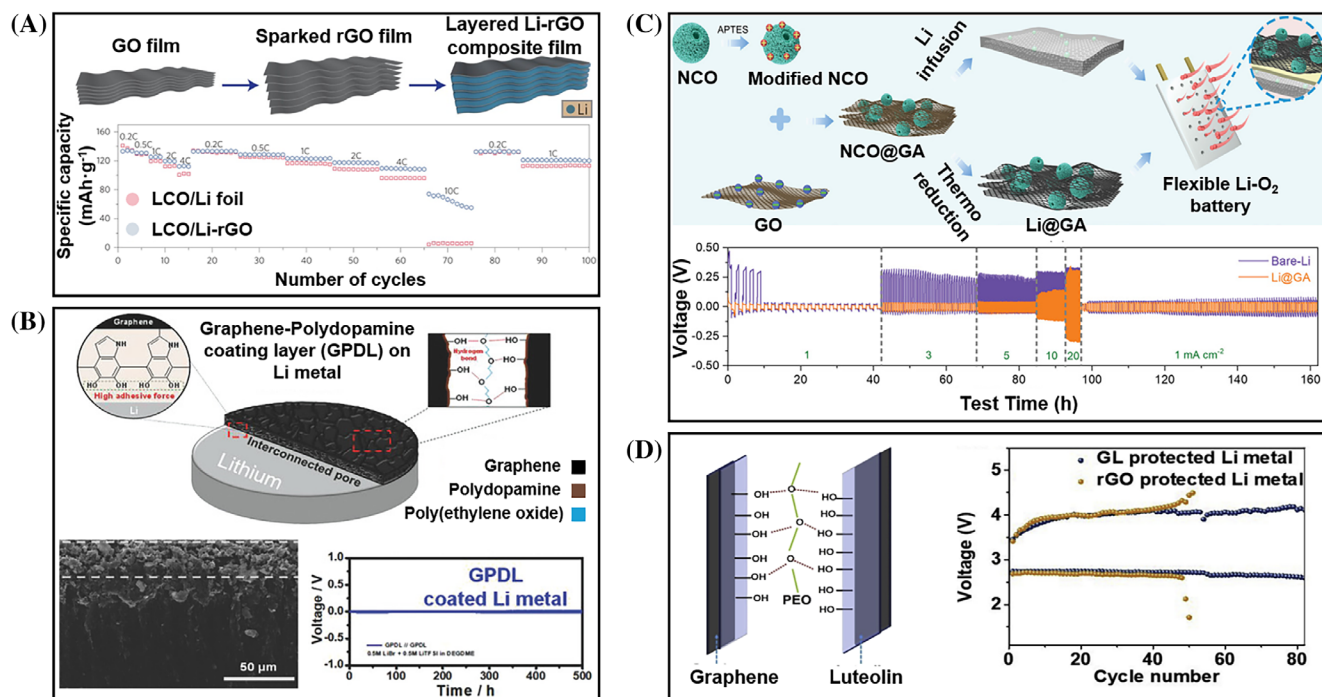


FIGURE 4 (A) Illustrations of the fabrication for a layered Li-rGO composite film and rate performance tests.⁸⁸ Reproduced with permission, Copyright 2015, Springer Nature. (B) Scheme of the coating process, cross-sectional SEM image, and Li plating/stripping results using an anode-anode symmetrical cell of GPDL.⁸⁹ Reproduced with permission, 2017, Wiley-VCH. (C) Schematic illustration of the synthetic procedures and rate performance tests under various current densities of Li-GA.⁹⁰ Reproduced with permission, 2020, Wiley-VCH. (D) Variation of charge and discharge terminal voltage of GL-protected and rGO-protected Li anode.⁹¹ Reproduced with permission, 2020, Elsevier

spark reaction occurred immediately across the whole film to construct a porous structure of the rGO film. The lithophilic nature of sparked rGO and the capillary force produced by the interlayers led to infuse Li homogeneously into the interlayer spacing yielding the Li-rGO composite anode, which indicates the excellent rate capability in LCO/Li-rGO cell at a high rate (110 mA h g⁻¹ at 4 C and 70 mA h g⁻¹ at 10 C). As illustrated above, porous carbon materials are effectively used as metal hosts due to their high surface area and 3D interconnected structure, which can increase metal concentration in anode and suppress the dendrite growth. Sun et al. also prepared the graphene-polydopamine (PD) coating layer on the surface of Li metal, as shown in Figure 4B.⁸⁹ Along with a superior physical and electrochemical properties of graphene, the PD with catechol groups in graphene/PD composite layer strongly combines with Li and H bonding with PEO binder, which can expedite Li-ion transfer and suppress the uneven growth of Li, thereby achieving the stable long-term cycling for Li-O₂ batteries. Also, Bobnar et al. observed the cyclic stability of the fluorinated rGO and Li composite (FGI@Li).⁹² The fluoro-functional group, which has been shown to have an ability to stabilize the capacity of Li-S batteries,^{93,94} effectively suppresses the side

reaction on the LAB anode, as observed by the XPS analysis that could monitor the ratio of irreversible Li₂O among discharge products. For the non-protected Li, the percentage of Li₂O from total Li anode increases from ~5% at 30th cycles to ~10% at 100th cycles. On the other hand, the percentage of the Li₂O in total FGI@Li anode remains ~1% after 100 cycles. Inspired by the positive effect of the hetero-element incorporation, the chemical approach to understand the uniform lithium nucleation with the lithophilicity of heteroatom doping is theoretically implemented.⁹⁵ By placing the non-metal elements on various sites of the graphene, the binding energy of the Li on the site could be estimated. As a result, both O doping and O/B co-doping are predicted to show the highest lithophilicity among other single- and co-doped carbons. Along with the overpotential test of Li nucleation, the lowest overpotential of O-doped graphene among pristine and N-doped graphenes indicates the lithophilicity as a key factor. As shown in Figure 4C, the role of the GO layer for enhanced cycle performance is investigated more detailed by Ma et al.⁹⁰ In comparison with the rate performances of the bare Li and GO aerogel embedding Li (Li@GA) anodes, the polarization becomes more severe for the bare Li anode at high current rates, while the Li@GA anode

shows comparatively mild polarization. The higher discharge/charge hysteresis of the bare Li at high current densities was attributed to the accumulation of thick SEIs and severe interference of the Li^+ diffusion by “dead” Li.⁹⁶ Moreover, the specific capacity of the Li@GA anode was measured by full Li-stripping. Upon charging to 1 V (vs. Li^+/Li) at 0.5 mA cm^{-2} , the specific capacity of $3398.4 \text{ mA h g}^{-1}$, or 88% of the theoretical capacity of pure Li (3860 mA h g^{-1}), was achieved for high energy density. Guo et al. also employed rGO/Li composites as anode and obtained a comparable result.⁹¹ The sufficient space for the Li deposition is associated with the plentiful void of the rGO/Li composite, while the growth of the dendritic Li is suppressed during the cycle. Furthermore, mechanical integrity is given to artificial SEI due to the flexible nature of the rGO, which endures the volumetric change upon cycling. As shown in Figure 4D, the cycle performance is improved with the addition of extra polymer.⁹⁷ Using the diphenyl picryl phenyl hydrazine (DPPH) added TEGDME electrolyte for the catalytic activity of battery, the composite of the rGO@luteolin (GL) was synthesized acting as a superior protective layer. The GO ink was used as carbon sources for the porous graphene architecture prepared by direct 3D printing. As-prepared hydrogel lattices were fully dried by using the freeze-dryer and heated at 250°C in an Ar atmosphere. With the addition of the DPPH, the nitrogen radicals were generated during the charging and discharging process and stabilized by the luteolin against the anode attack. In addition, the luteolin on the surface of rGO could form stable quinoid radicals with DPPH. Eventually, the incorporation of the luteolin increases the lifetime of the battery, by suppressing the Li dendrite growth and reducing the oxidation of DPPH electrolyte, resulting in a specific capacity of 1000 mA h g^{-1} at the current density of 400 mA g^{-1} and a low terminal charge potential (4.12 V) after 80 cycles.

3.2 | Disordered carbon nanomaterials

Disordered carbon nanomaterials have drawn much attention owing to their facile preparation, including the pyrolysis of polymer precursors and the catalytic graphitization at relatively low temperature, as well as higher surface area and easier surface modification compared to the synthesis process of graphitic carbon materials. Despite these advantages of disordered carbon materials, the hybridization of ordered and disordered carbon materials with heterogeneity is the key to design the optimized structure, providing the partial graphitic domains with high electrical conductivity and chemical stability for the

amorphous carbon materials. In sharp contrast to the synthesis of ordered carbon materials from fossil fuel species at high temperatures, the pyrolysis of organic materials or biomass induces the formation of disordered carbon materials. For instance, Cui et al. prepared the hollow carbon spheres with polystyrene templates through the pyrolysis process for application into Li metal hosts, as shown in Figure 5A. These amorphous hollow carbon layers can provide the chemical stability the fast charge transfer, the suppression for the formation of Li dendrite, and the stable SEI for Li metal.⁹⁷ As shown in Figure 5B, Zhang et al. reported the uniformly N-doped hollow carbon nanospheres as Li metal hosts. Such the functionalized carbon nanospheres with lithophilic nitrogen lead to the mitigation of local current density and Li dendrite growth and the uniform electrodeposition of Li metal.⁹⁸ Moreover, the voids within hollow carbon structure could regulate the volume expansion during the Li plating/stripping. On the other hand, Tao et al. demonstrated the facile synthesis of biomass-derived porous carbon nanosheets with S and N elements doping for the application as Li metal hosts, as shown in Figure 5C.⁹⁹ The chitosan, gelatin, and thiourea can be used as carbon precursors and doping sources of disordered carbon materials, respectively. The elemental S and N co-doping is effective for the nucleation of Li metal as verified by the experiments and theoretical calculation. Li@SNC sample with S/N ratio of 1 showed the best cycling performance. For Li without carbon, the cycle stability is preserved for 500 h, while the Li with carbon is stable over 1500 h. While the Li with undoped carbon showed gradual increase in hysteresis over cycles, Li@SNC sustained the voltage fluctuation for 1500 h. When the binding energy with Li was calculated from the first principle calculations, the SNC had the strongest interaction with Li due to the synergetic effect of S and N elements through the p-orbital hybridization. Qian et al. also prepared the elemental N and O co-doped carbon materials on Cu foam derived from metal-organic frameworks through the one-pot vacuum pyrolysis. As can be seen from the Li plating scheme in Figure 5D, the presence of the N/O dual-doped 3D porous carbon architectures (NOCA) on Cu foam (CF) leads to the uniform deposition of the Li at the anode, which prevents the dendrite growth.¹⁰⁰ The coulombic efficiency of NOCA@CF was maintained over 600 cycles, while pristine Cu foam was stable only for 150 cycles. Even in the carbonate-based electrolyte, much more corrosive than ether-based electrolyte, NOCA@CF sustains the coulombic efficiency for 300 cycles. Various ordered/disordered carbon materials for metal hosts in LABs with synthesis methods and their electrochemical performances are summarized in Table 1.

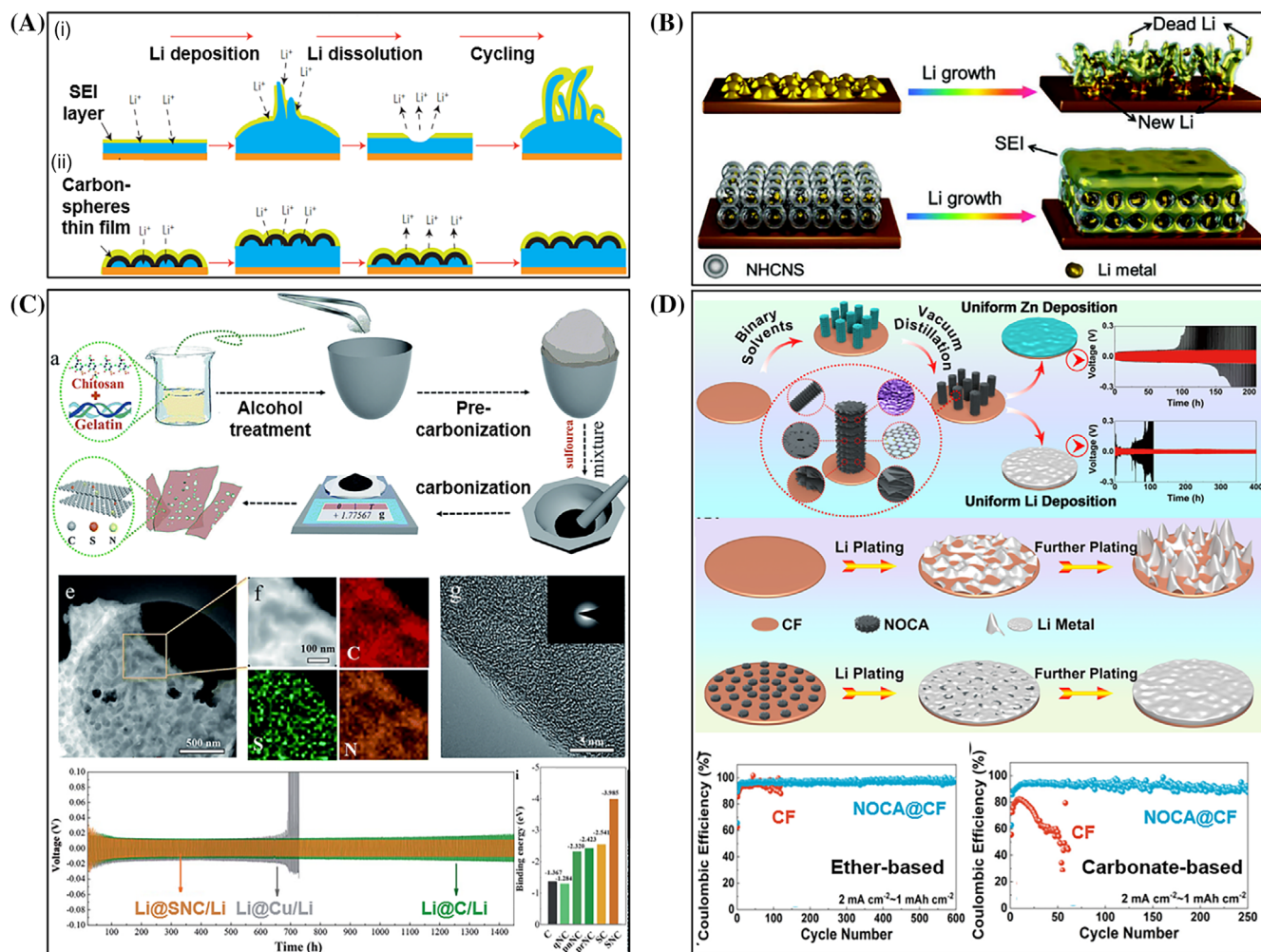


FIGURE 5 (A) Schematic illustrations for (i) direct pristine Li deposition on Cu substrate; (ii) Modification of the Cu substrate with a hollow carbon layer.⁹⁷ Reproduced with permission: Copyright 2014, Springer Nature. (B) Schematic description of Li growth on Cu foil and 3D NHCNSs host.⁹⁸ Reproduced with permission, Copyright 2020, Wiley-VCH. (C) Schematic illustration of the SNC synthesis, STEM image of a SNC, and Galvanostatic cycle performance of symmetric Li/Li@C, Li/Li@Cu, and Li/Li@SNC.⁹⁹ Reproduced with permission, Copyright 2019, Royal Society of Chemistry. (D) Schematic illustrations for the fabrication of NOCA@CF, metal deposition on CF and NOCA@CF, and Electrochemical properties of CF and NOCA@CF in carbonate-based electrolyte for Li metal anode.¹⁰⁰ Reproduced with permission, Copyright 2020, Elsevier

3.3 | Graphitic carbonaceous nanostructures for cathode

The electronic and porous structure of the electrocatalysts is regarded as the crucial factor for the design of cathode materials. Since the large accessible surface area of the cathode is associated with an increased number of reaction sites, the electrocatalytic activity can be enhanced to deliver high capacity. Furthermore, the discharge process of the LAB accompanies the precipitation of insoluble Li_2O_2 in nonaqueous electrolyte on the cathode. When the catalyst surface on the cathode is fully covered by insulating Li_2O_2 , however, there is a stiff drop of cell potential, as the charge transfer for additional discharge reaction is hindered.

The nanostructured graphene is a promising candidate to provide the large surface area and high electronic conductivity of the carbon material. Sun et al. compared with the commercial Vulcan XC-72 carbon and graphene nanosheets (GNSs).¹¹² The Vulcan XC-72 carbons show the morphology of agglomerated particles, whereas GNSs reveal the wrinkled structure. As verified by the N_2 adsorption-desorption isotherms, the specific surface areas of Vulcan XC-72 carbon and GNS derived from Brunauer-Emmett-Teller (BET) method are 240 and 309 $\text{m}^2 \text{g}^{-1}$, respectively. To maximize the accessible surface area, Xiao et al. presented hierarchical structure of the graphene as shown in Figure 6A. The inset SEM image shows the morphology of the loosely packed, broken egg structures of synthesized LAB cathode material.¹¹³ To construct this

TABLE 1 Summary of nanostructured carbon hosted anode materials for Li-air batteries

Metal host	Synthesis method	CE [mA cm ⁻²]/[mA h cm ⁻²]	Cell performance [mA cm ⁻²]/[mA h cm ⁻²]	Refs.
Stacked rGO	Hydrothermal method	97.1% for 200 cycles, 0.5/1	1500 h/1/0.5 0.5	101
Crumbled rGO ball	Aerosol-assisted capillary compression method	97.5% for 700 cycles, 0.5/0.5	750 h/0.5/1	102
Porous CNT	CVD method	96.0% for 200 cycles, 0.5/0.5	200 cycles/0.5/0.5	103
CNT paper	A floating catalyst CVD method	97.5% for 100 cycles, 5/1	2000 h/10/10	104
CNT/PANI	Vacuum filtration	-	550 h/0.5/0.5	105
Graphitized CF	Purchased from company	98% for 50 cycles at 0.5/8	300 h/2/2	106
Li-CF	Rolling method	98.5% for 100 cycles, 1/3.25	1000 h/1/1	107
N-doped rGO	CVD method	96.0% for 200 cycles, 0.5/1	1450 h/1/1	108
S/N co-doped carbon	Thermal reduction	98% for 250 cycles at 1/1	1500 h/1/5	99
Wood-derived carbon	Pyrolysis method	-	450 h/1/1	109
3D carbonized wood	Pyrolysis method	-	150 h/3/1	110
Amine-functionalized CF	Pyrolysis method	91% for 200 cycles at 1.33/4	over 4000 h/1.56/6.32	111

Abbreviations: CE, Coulombic efficiency; CF, carbon fiber; CNT, carbon nanotube; CVD, Chemical vapor deposition; rGO, reduced graphene oxide/graphene.

structure, the functionalized graphene sheet (FGS) produced by the thermal expansion and simultaneous reduction of graphene oxide, which provide the carboxyl functional group, was used as the base material. After dispersing the FGS in a microemulsion solution containing binder material, through the casting and drying, the aforementioned morphology can be constructed. The formation of broken egg morphology is attributed to the bubbles, arising from the mixing of aqueous polytetrafluoroethylene (PTFE) with FGSs, where the skin of the bubble is surfactant-rich interacting with the hydrophobic surface of FGS. With the enhanced reaction kinetics by generated carboxyl functional groups, the unique structure of FGS enables to give a superior specific surface area of 590 m² g⁻¹, which leads to the specific capacity of ~5000 mA h g⁻¹ under 0.1 mA cm⁻² in the ambient air.

Porous structure is also a crucial factor to affect the reaction kinetics in the cathode. Because the charge/discharge reaction of the LAB takes place at the interface of two different phases, so-called electrolyte (solid or liquid) and oxygen (gas) phases, the cathode should provide a proper channel for the mass transport of reactants and products. Furthermore, the discharge product, when precipitated at the surface of cathode material, in some cases, can block the channel for oxygen transport, thereby interfering with the recharging reaction on the remaining surfaces of the cathode for the capacity fading. As displayed in Figure 6B, the hierarchical architected carbon with the macrochannel and mesopores is designed.¹¹⁴ The macrochannel with ~150 nm is derived from the stacked nanoslices composed of graphene sheets, while the

mesopore of ~40 nm is distributed within the nanosheets. The mesopore is formed during the thermal treatment process of the sol-gel synthesis of the carbon architecture. Each macrochannel and mesopore plays its respective role during the charge/discharge process: The macrochannel facilitates the O₂ and electrolyte diffusion through the transporting pathway and the mesopore contributes to the rapid transport of Li⁺ ions and the storage site for the discharge product. Zhou et al. also obtained the hierarchically mesoporous/macroporous graphene through the vacuum-promoted thermal expansion,¹¹⁹ where a pressure of 0.1 bar is exerted to GO followed by heating at 900°C.¹²⁰ Promoted from the open porous structure with large surface area, graphene cathode exhibited a high capacity of 19 800 mA h g⁻¹. Zhong et al. designed the 3D graphene membrane for the highly porous carbon cathode.¹²¹ Using GOs obtained from Hummer's method, 3D architecture was created through a freeze-drying process. As the small pieces of GOs cannot construct a highly dense 3D structure, the size of GOs is strictly controlled to ~1 μm. In particular, the as-synthesized graphene membrane allows LABs to exceeds 5700 mA h g⁻¹ of the maximum cathode capacity.

To obtain the maximized surface area and optimal channel for the reactant transport, Lim et al. designed the woven structure CNT as presented in Figure 6C.¹¹⁵ According to the cyclability profile, the initial specific capacity of the woven CNT is near 2500 mA g⁻¹, whereas that of CNT powder is around 1000 mA g⁻¹. In sharp contrast to the deep discharge to 2 V directly deteriorates the capacity of the CNT powder; no significant degradation was observed for the woven CNT up to 20 cycles.

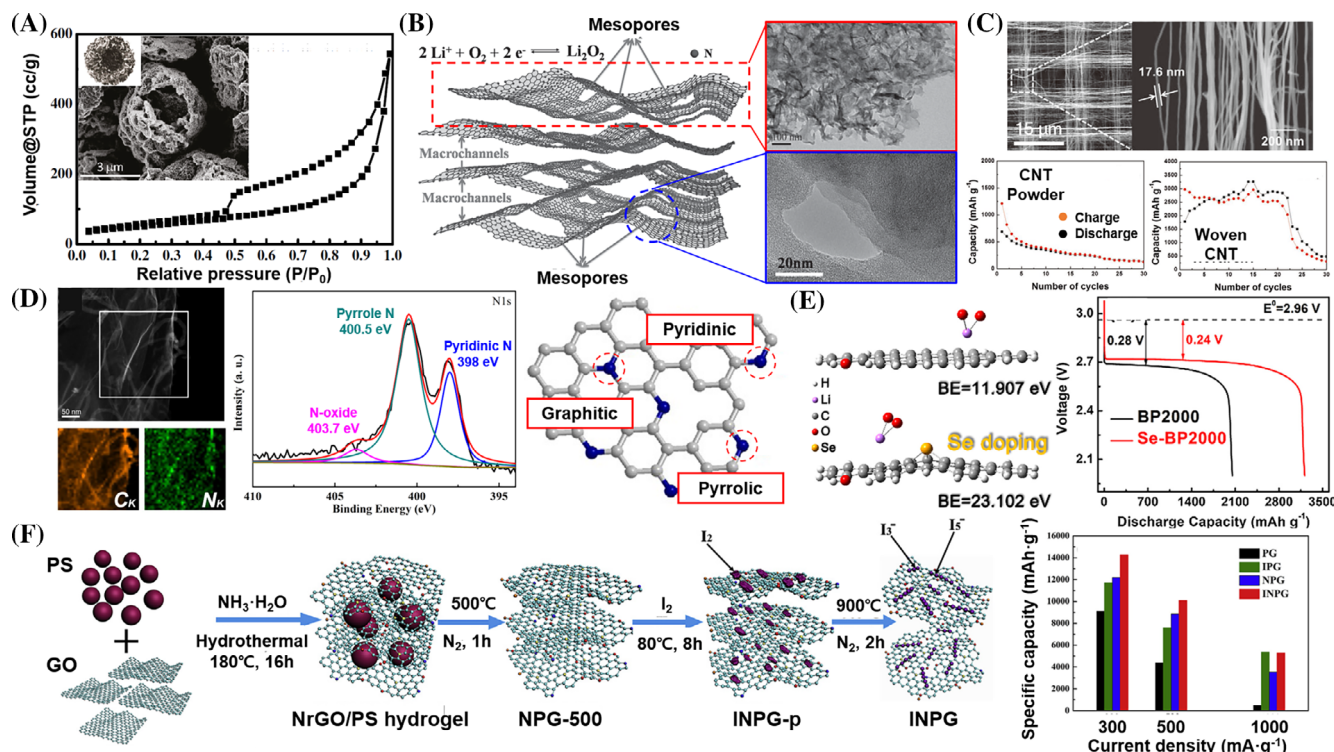


FIGURE 6 (A) The N₂ adsorption isotherm of the FGS based air electrode.¹¹³ Reproduced with permission, Copyright 2011, American Chemical Society. (B) Scheme illustration of hierarchical carbon-nitrogen with the TEM images of microchannels and mesopores.¹¹⁴ Reproduced with permission, Copyright 2014, Wiley-VCH. (C) SEM images of the pristine and discharged CNT fibril with cyclabilities of CNT powder and woven CNT.¹¹⁵ Reproduced with permission, Copyright 2012, Wiley-VCH. (D) STEM image, elemental mapping of C and N with scheme of various doped nitrogens.¹¹⁶ Reproduced with permission, Copyright 2015, Wiley-VCH. (E) The optimized geometries of LiO₂ binding on BP-2000 and Se-BP-2000 with discharge curve. Reproduced with permission, Copyright 2020, Elsevier.¹¹⁷ (F) Schematic illustration for the synthesis of INPG and specific capacity.¹¹⁸ Reproduced with permission, Copyright 2019, Elsevier

For the CNT powder, the deep discharge to 2 V leads to the aggregation of discharge product, which substantially increases the resistance of the electrode. Accordingly, such a resistive electrode results in severe polarization, which is detrimental to the cycle life and energy efficiency.¹²² On the other hand, the open framework of woven CNT allows the discharge product to be deposited uniformly onto the cathode surface. This uniform distribution of discharge products is beneficial for inhibiting the partial clogging in the electrode surface to promote the reaction kinetics.

The surface modification is another strategy for the high activity of carbon materials. Because the pristine graphene is not sufficiently active for ORR or OER during the charge/discharge process, substantial efforts have been devoted to modify the surface of graphitic carbons through various methods. One method is the incorporation of heteroatoms such as a nitrogen, sulfur, iodine, or even metal elements. Nitrogen atoms with a similar size to carbon were incorporated into the graphene and graphene/CNT hybrid, where the structure distortion is minimized. Moreover, the lone pair electron of the N

atom increases the electrical conductivity of carbon material.^{123,124} As shown in Figure 6D, the introduced N atoms are uniformly dispersed throughout the whole range of graphene.¹¹⁶ According to the XPS data, three types of N atoms, such as pyridinic, pyrrolic, and graphitic N, are verified depending on the local binding with adjacent carbons. Each nitrogen has different catalytic activities toward the OER/ORR. Representatively, pyridinic N is known to have high reactivity toward lithium oxidation, while graphitic N enhances the conductivity of carbon. To optimize the activity of N-doped carbon, Sakaushi et al. tried to control the portion of various nitrogens.¹²⁵ By elevating the temperature of thermal treatment of precursors from 900 to 1000°C, the amount of pyridinic N decreased, whereas the proportions of the other two nitrogens increased. Consequently, the bifunctional catalytic activity was irrelevant to the portion of various nitrogens, whereas the stability is proportional to the amount of graphitic N. The reactivity of various types of N atoms for the discharge reaction has been controversial. Yun et al. compared the catalytic activity of the pyridinic N site and graphitic N site through the DFT

calculation.¹²⁶ By comparing the formation energy of discharge products on various nitrogen sites, the graphitic nitrogen site acts as a more favorable site for the lithium oxidation reaction to occur rather than the pyridinic nitrogen site. The Bader charge analysis indicates that the carbon atoms adjacent to the graphitic N site become an effective catalytic mediator by transporting charge from the surface to the reaction intermediate. On the other hand, Jing and Zhou demonstrated the opposite tendency for the catalytic activity of graphitic and pyridinic N.¹²⁷ Based on the single graphitic, pyrrolic, and pyridinic N site in the graphene, even more complex active sites composed of multiple N atoms are modeled. For each model, the free energy of the Li_4O_4 formation is calculated. The reaction barrier is confirmed from the calculation and the Li_4O_4 formation at the site composed of 4 pyridinic N shows the lowest reaction barrier, which reveals the catalytic activity of pyridinic N. The comparison of the chemical doping effect between different dopant elements is also implemented by Han et al.¹²⁸ Based on the nanoporous graphene, each S and N are adopted as the dopant. While the N-doped graphene gives the rise to an extremely large discharge capacity of $10\,400\text{ mA h g}^{-1}$, twice than that of S-doped one, S-doping stabilizes the cycling behavior with its moderate degradation rate. To benefit from both dopant elements, Kim et al. synthesized the S, N dual-doped mesoporous carbon on graphene.¹²⁹ Nourishing the synergetic effect of S and N dopant, S depresses the degradation rate, leading to the cyclability over 100 cycles, whereas N provides the gravimetric capacity over $11\,000\text{ mA h g}^{-1}$.

Besides nitrogen, active single atom species have received significant attention in the design of bifunctional catalysts. The scheme of the LiO_2 adsorption on Se-doped carbon is depicted in Figure 6E. As shown in the discharge curve, the discharge capacity of Se-doped carbon was dramatically enhanced facilitating the kinetics of oxygen involving reaction.¹¹⁷ Such improvement in the reaction kinetic is closely related to the size of the Se atom. Because the Se atom has a larger diameter than C, the incorporation of the Se into carbon brings the distortion of the local structure. The strain in the carbon structure promotes the charge localization and attracts the oxygen chemisorption, boosting the ORR catalytic activity.¹³⁰ In addition to the favorable reaction kinetics, the Se dopant efficiently alleviates the side reactions, enhancing the stability of the cathode. As the Se compounds act as superior antioxidants by scavenging the free radical effectively, the side reaction caused by the superoxide radicals on the cathode can be suppressed with doped Se.^{131,132}

Beyond the single doped graphene for the cathode, Wu et al. presented N and I dual-doped graphene as

bifunctional catalysts for LAB cathodes.¹¹⁸ As depicted in Figure 6F, the nitrogen is firstly introduced through the hydrothermal process with ammonium hydroxide. After drying and annealing to decompose the polystyrene spheres, they are mixed with I_2 and mildly heated for the precursor formation. Then, the resulting precursor is heated at 900°C to achieve uniformly dual-doped porous graphene. With the multielement co-doping, the doped I atom affects the bonding configuration of the active sites by breaking the electric neutrality of the sp^2 carbon, which enhances the intrinsic activity for O_2 adsorption and reduction.

Although the breaking of sp^2 carbon structure enhances intrinsic activity, it also deteriorates the stability of the carbon structure. Yoo et al. investigated the influence of the proportion of sp^3 and sp^2 carbon on the electrochemical performance of the GNS cathode.¹³³ The increase in the sp^2 carbon and the decrease in the sp^3 carbon for CNT are attributed to the graphitization of basal plane during the heat treatment, as the sp^3 carbon is mainly derived from the edge site or the defect. According to the discharge overpotential along with cycles, the heat-treated, highly graphitized, GNS possesses higher overpotential due to the loss of reactive defect sites and functional groups but bares twice more cycles than high sp^3 concentration GNS.

The correlation between the crystallinity of the carbon and cyclic stability is studied by Bae et al.¹³⁴ As the cathode degradation during the charge/discharge cycle is mainly derived from the side reaction, which decomposes the electrolyte and carbon electrode, it is possible to analyze the degree of degradation estimating the amount of CO_2 evolution. In order to distinguish the carbon of the cathode from that of the electrolyte, the carbon atoms of air electrodes are replaced with the carbon isotope ^{13}C . The crystallinity of the carbon is controlled varying the heat-treatment temperature from 1600 to 2800°C , where higher crystallinity is obtained at higher temperatures. As demonstrated by the in situ differential electrochemical mass spectroscopy (DEMS), the highly crystalline carbon cathode generates less amount of CO_2 , especially for $^{13}\text{CO}_2$. Thus, this finding elucidates that the high-crystalline carbon is capable of achieving superior rechargeability by suppressing the side reaction owing its electrochemical stability.

3.4 | Non-graphitic carbonaceous nanostructures for cathode

Due to the comparatively low crystallinity, the cathode with non-graphitic carbonaceous nanostructures has the stability issue. To overcome this limitation, various

approaches to obtain stability have been developed. Moreover, in a similar manner to graphitic carbons, investigations toward hierarchical structure and enhanced intrinsic activity are also underway.

To achieve maximized surface area, Li et al. controlled the activation process of the carbon cathode by using different activators.¹³⁵ In Figure 7A, each sample denominated as CA, CB, and CC is synthesized with the chitin precursor and chemically activated with H_3PO_4 , KOH, and KHCO_3 , respectively. The CA is featured with the open-cluster channel structure composed of the piled-up spherical cluster, while CB and CC achieve honeycomb macropore structure with different pore sizes. The spherical cluster structure of CA with a large surface area of $753.74 \text{ m}^2 \text{ g}^{-1}$ is associated with the activation process with H_3PO_4 , which inhibits the unstable volatilization of the carbon in the course of carbonization.¹³⁹ Unlike the H_3PO_4 , KOH and KHCO_3 go through the decomposition process during the heat treatment to generate the gas species during the carbonization and generated gas leads to the honeycomb macropore structure of CB and CC.¹⁴⁰ Among samples, CA showed the highest discharge voltage of 2.76 V and specific capacity of 8400 mA h g^{-1} . As presented in Figure 7B, vertically aligned N-doped coral-like carbon fiber is synthesized by

the CVD method.¹³⁶ With the pyrolyzed iron phthalocyanine (FePc) source, the mixture of helium and hydrogen is used as the carrier gas to grow the vertically aligned coral-like carbon fibers. In comparison to common carbon fibers of CNT, vertically aligned N-doped coral-like carbon fiber maximizes the surface area owing to abundant branches along the main fiber. Along with the alignment effect, the overpotential decreased for both charging and discharging to the large extent. The method to control the surface area of disordered carbon particles was investigated by Li et al.¹⁴¹ During the heat treatment under NH_3 gas, the gasification reaction of the carbon black occurs to increase the surface area by pore generation. Pyrolysis process mainly generates the mesopore in carbon black, providing the specific surface area of $\sim 1200 \text{ m}^2 \text{ g}^{-1}$, and the large surface area leads to specific capacity of 5000 mA h g^{-1} , whereas carbon black without mesopore possesses 1000 mA h g^{-1} .

The heteroatoms are generally incorporated into the ordered carbons through the post-treatment. By contrast, the heteroatoms are well dispersed onto the surface of disordered carbons through the direct pyrolysis of the dopant-containing materials. MOF is one base material for the design of carbon structure.¹⁴² Meng et al. derived the Ru-incorporated carbonaceous LAB cathode from the

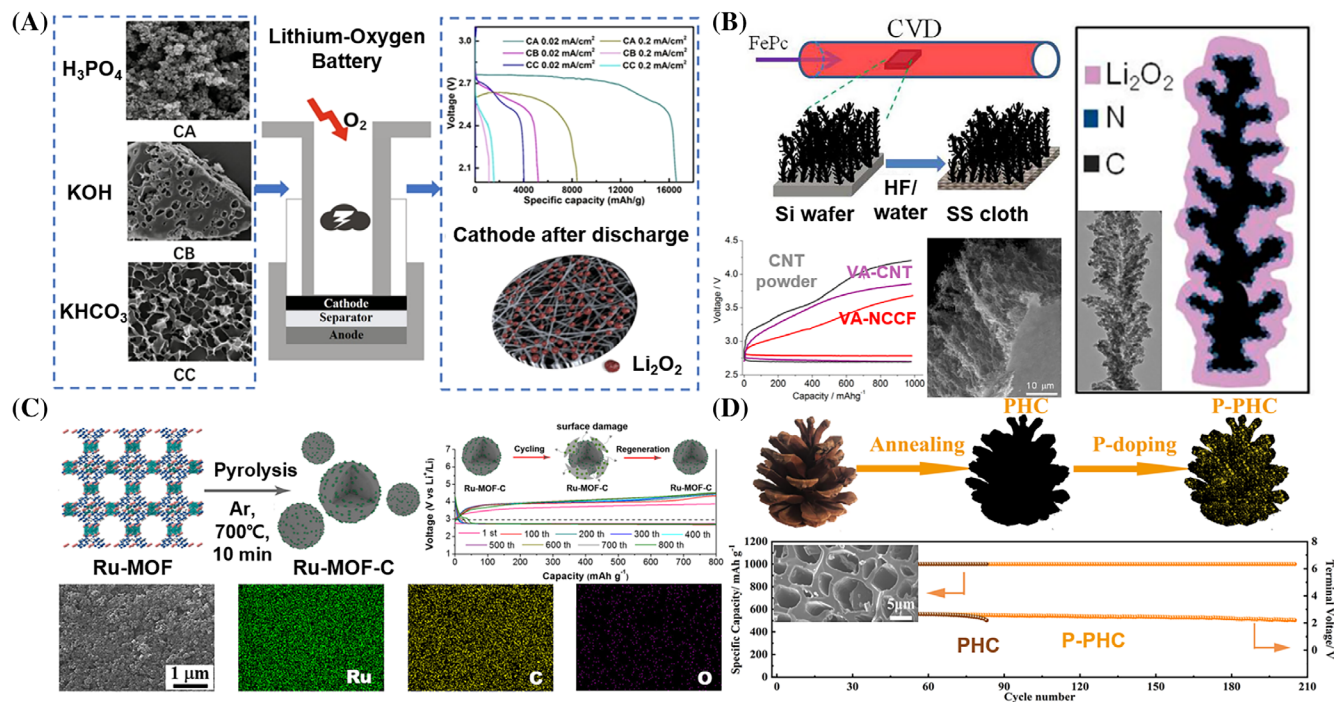


FIGURE 7 (A) Scheme of the synthesized carbon cathodes with various morphology through three activators and nitrogen adsorption-desorption isotherms of CA.¹³⁵ Reproduced with permission, Copyright 2019, American Chemical Society. (B) Scheme of the synthesis process of the VA-NCCF and SEM, TEM images of synthesized nanofibers.¹³⁶ Reproduced with permission, Copyright 2014, American Chemical Society. (C) Schematic illustration of the fabrication process of Ru-MOF-C and SEM image with EDS mapping.¹³⁷ Reproduced with permission, Copyright 2019, American Chemical Society. (D) Schematic illustration of the preparation of PHC, P-PHC with SEM images and cyclic performance.¹³⁸ Reproduced with permission, Copyright 2019, American Chemical Society

metal–organic framework (Ru-MOF-C) as shown in Figure 7C.¹³⁷ In the study, MOFs are constructed with RuCl_3 secondary building unit and benzenetricarboxylic acid organic linker and used as the precursor for carbonization. The as-incorporated Ru is well scattered throughout the whole portion of carbon structure without any aggregation and sustain much stronger adhesion with the carbon structure when compared to Ru particles decorated through other deposition methods. The pyrolysis of the MOF provides the cathode with better electrochemical stability in spite of the low crystalline carbon nanostructure. The discharge capacity of Ru-MOF-C kept stable over 800 cycles, whereas that of CNT decreased to ~85% of initial capacity after 100 cycles. Hu et al. also synthesized Ru single atom-loaded cathode by the pyrolysis of Zn containing MOF.¹⁴³ At 900°C, Ru is introduced to the Zn site, combining with near nitrogen atoms. By controlling the amount of Ru, the discharge overpotential reached the value of 0.17 V. Wang et al. presented the atomically dispersed cobalt catalyst anchored on N-doped carbon nanosheets.¹⁴⁴ Through the green gas-migration-trapping strategy, Co single atoms are embedded on the pyridinic N site in the form of Co-N_4 . The Co-N_4 species distributed in the carbon structure act as the active catalytic centers, which contribute to the decomposition kinetics of the Li_2O_2 . Compared to carbon with Co nanoparticles, the total overpotential for the charge and discharge decreased from 1.02 to 0.4 V, mainly due to the enhanced LiO_2 -absorption ability and modulated growth process of Li_2O_2 .

In a similar manner to MOF-derived carbon, Nong et al. derived an N-doped carbon framework from the carbonization of 3D ultra-lightweight polyaniline (PANI).¹⁴⁵ The 3D structure of the PANI is constructed by coating PANI on the PMMA template and removing PMMA. As analyzed by the XPS spectra, the proportion of the pyridinic and graphitic carbon varies with the temperature of carbonization. With increasing temperatures, a portion of the graphitic carbon was raised, which is favorable for enhancing catalytic activity. A simple method to prepare P-doped pinecone-derived hive-like carbon (P-PHC) is represented in Figure 7D.¹³⁸ As derived from the wood-like biomass, its water delivery is associated with the 3D porous structure, which provides a suitable pathway for oxygen transport during the reaction. Furthermore, P-doping through the hydrothermal process generates extra active sites that are favorable for the charge transfer to reaction intermediates. The incorporated P in the carbon also enhances the chemical stability of the nanostructure. As shown in Figure 7D, the incorporation of P improves the capacity retention of nearly 100% over 200 cycles twice than that of PHC. Multiple heteroatom-doped carbon is also synthesized

through the carbonization of the biomass. Jo and Ahn synthesized N, P co-doped porous-activated carbon from the carbonization of protein-based tofu.¹⁴⁶ During the decomposition of amino acid by carbonization, N-doped carbon is formed as followed by the extra P-doping through high-temperature calcination. In particular, nitrogen atoms increase the electron distribution on the electrode, while phosphorus atom bonds with oxygen, forming the oxygen-containing group at the edge of graphite lattice, which both of them improves the catalytic activity.

The density of the oxygen functional group also affects battery performance. Lee et al. investigated the influence of the oxygen functional group on the reaction kinetics of Li_2O_2 formation by modifying the porous carbon nanowebs (PCN).¹⁴⁷ Simply varying the heat-treatment temperature of the PCNs, carbon surface can be successfully modified, while other factors such as the surface area or pore sizes almost remain intact. At the high temperature of 2800°C (PCN2800), the atomic ratio of the oxygen and carbon components (O/C) is 1.08, lower than 16.18 of PCN800 treated at 800°C. Moreover, the oxygen functional group acts as the favorable site for the Li adsorption, where the formation of Li_2O_2 is promoted.¹⁴⁸ If the adsorption with Li is not sufficiently strong, reaction intermediate of LiO_2 is easily detached from the carbon, then the deprotonation reaction proceeds in the electrolyte, so-called the solution-mediated process. The solution-mediated process produces relatively large particles of Li_2O_2 . On the other hand, strong attraction of oxygen functional group with Li tends to be dominated by the surface-driven process, forming the film-like morphology to make the decomposition facile.^{149,150} Additionally, oxygen functional groups have an effect on the wettability of the electrode with electrolyte. The contact angle of each sample decreases as the heat-treatment temperature increases, as demonstrated by 74° and 30.4° for PCN2800 and PCN800, respectively. The high wettability of the PCN800 is mainly due to the hydrophilicity induced by oxygen functional groups. Considering that the active sites of carbon surface can be available when it is sufficiently wetted by the electrolyte, oxygen functional groups can promote the reaction.

3.5 | Metal-free carbon/carbon composite for cathode

In order to compensate for the limitation of single carbon-based material as cathode, complementary or synergistic carbon materials are incorporated into the carbon matrices through the composite formation. Especially, metal-free carbon/carbon composites have significant

advantages in terms of the high specific capacity arising from the light weight of carbons and abundant surface chemistries.

Luo et al. presented the composite of macroporous graphene and graphitic C_3N_4 (g- C_3N_4) for the bifunctional cathode material.¹⁵¹ As shown in Figure 8A, the composite air electrode is obtained through the two steps, using the hydrothermally synthesized GNS and C_3N_4 as precursors. Firstly, the self-assembly occurs in the hydrazine hydrate solution of graphene and C_3N_4 mixture through the heating process. Then, the macroporous structure of composite is created through the freeze-drying dehydration. For the composite, C_3N_4 provides the oxygen electrocatalytic activity in an analogous manner to the N-doped graphene.^{155–157} Compared to N-doped graphene with relatively low nitrogen contents and leaching of the nitrogen in the structure,¹⁵⁸ g- C_3N_4 is much more stable allotrope of N-carbon structures with rich N-sites. Because the electric conductivity of the C_3N_4 can be compensated by conductive GNSs, the composite electrode maximized the catalytic activity of the g- C_3N_4 .

As shown in Figure 8B, the composite of g- C_3N_4 and disordered carbon paper is synthesized simply dipping the carbon paper to the precursor solution and treating calcination process.¹⁵² Synthesized composite has much enhanced capacity of $\sim 450 \text{ mA h g}^{-1}$, compared to $\sim 50 \text{ mA h g}^{-1}$ of the single carbon paper. Figure 8C presents the synthesis process of the cathode composed of mixed polymer nanofibers with high CNT loading. Using the mixture solution of PAN, polyvinylpyrrolidone (PVP), and CNT, the electrospun sheet is achieved.¹⁵³ Then, a cathode can be fabricated through the simple washing with the water and the subsequent drying process. During the washing process, the domain occupied by the PVP is converted to the surface pore, while the remaining PAN domain forms the mechanical backbone for the nanofibers. The high amount of CNT, 65.8% of the polymer weight, is simultaneously deposited on the nanofiber, imparting the electrical conductivity to the matrix. As the PVP polymeric support promotes the facile ionic diffusion from electrolyte-containing fiber through the generated pore, it is possible to reach the specific

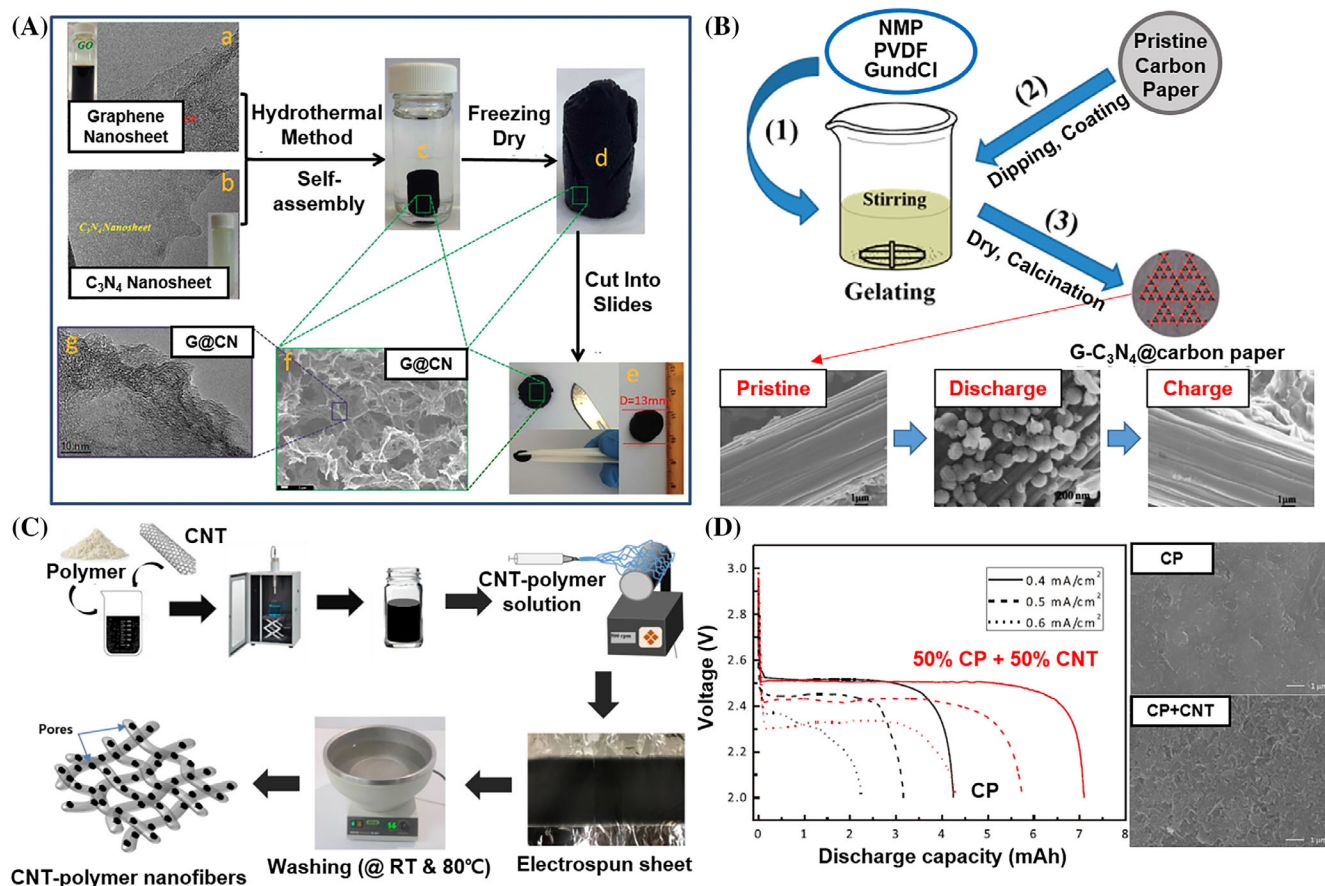


FIGURE 8 (A) Schematic flow-process diagram of the G@CN composite fabrication.¹⁵¹ Reproduced with permission, Copyright 2015, Wiley-VCH. (B) Routes for the facile in-situ preparation of g- C_3N_4 @carbon paper with SEM images of pristine, discharged and charged cathode.¹⁵² Reproduced with permission, Copyright 2015, American Chemical Society. (C) Synthesis of CNT-polymer composite nanofibers through electrospinning.¹⁵³ Reproduced with permission, Copyright 2020, Elsevier. (D) Discharge curve and SEM images of carbon powder and carbon powder-CNT composite.¹⁵⁴ Reproduced with permission, Copyright 2014, Elsevier

capacity of 4800 mA h g^{-1} , much improved from 1500 mA h g^{-1} of CNT-PAN.

As revealed by Figure 8D, the discharge curves of the carbon powder cathode and carbon powder-CNT composite cathode are compared.¹⁵⁴ As the discharge current density increases from 0.4 to 0.6 mA cm^{-2} , the capacity retention of the composite is 60.4% , while that of carbon powder is 52.8% . This result indicates the better rate performance of the composite cathode. In addition, the composite provides the porous structure, as seen in the SEM images.^{151,153} Thus, composite achieved the volumetric/gravimetric capacity of $258.06 \text{ mA h cm}^{-3}$ and $779.14 \text{ mA h g}^{-1}$, 67.2% and 36.3% higher, respectively, than densely packed carbon powders. Various ordered/disordered carbon materials for cathode in LABs with synthesis methods and their electrochemical performances are summarized in Table 2.

3.6 | Full-cell measurements with carbonaceous electrodes

For the practical applications, the full-cell measurements have been performed to demonstrate the feasibility of the as-designed electrodes for LABs. Sun et al. obtained the

performances of Li-O₂ cells to confirm the effect of GPDL on Li metal, compared to pristine Li metal.⁸⁹ In Figure 9A, GPDL-coated Li metal electrode indicated the remarkably stable discharge and charge profiles, which showed the upper potential plateau with a better stability in discharge profiles, compared to bare Li metal. Moreover, SEM images of GPDL-coated and pristine Li metal electrodes after 200th and 15th cycles, respectively, exhibited the clear difference of dendrite formation, resulting to the stable long-term cycling of GPDL-coated electrode. Li and Manthiram presented the O- and N-doped carbon nanoweb (ON-CNW) for the metal-free bifunctional cathode catalysts.¹⁵⁹ To evaluate the OER and ORR activities of the ON-CNW, N-doped carbon nanosphere (N-CNS) and N-doped carbon nanoweb (N-CNW) samples are also prepared for comparison. As evaluated by the half-cell measurement with saturated calomel electrode (SCE, vs. Hg/HgO), the lowest overpotential for the ORR was observed for the ON-CNW. To confirm the feasibility of the practical battery application, the full-cell test was carried out using the cell with polytetrafluoroethylene (PTFE) layered battery mold as shown in Figure 9B. From the discharge voltage profile, the discharge plateau of ON-CNW is only 0.077 V lower

TABLE 2 Summary of nanostructured cathode materials for Li-air batteries

Cathode material	Synthesis method	1st discharge capacitance [mA h g^{-1}]/[V]	Cyclic performance [mA h g^{-1}]/[mA h g^{-1}]	Refs.
Porous carbon nanoweb	Freeze-drying and heat treatment	$25\,555 \text{ mA h g}^{-1}$ $0.2 (\text{mA cm}^{-2})/2.0$	80 cycles $0.2 (\text{mA cm}^{-2})/500$	147
Woven CNT	CVD	$\sim 3000 \text{ mA h g}^{-1}$ $2000/2.0$	80 cycles $2000/1000$	115
Vertically aligned Carbon Fiber	Pyrolysis method	$\sim 40\,000 \text{ mA h g}^{-1}$ $500/2.2$	200 cycles $250/500$	136
Meso/microporous graphene	Vacuum-promoted thermal expansion	$19\,800 \text{ mA h g}^{-1}$ $300/2.0$	50 cycles $1000/1000$	119
S-doped Graphene	CVD	4920 mA h g^{-1} $200/2.3$	300 cycles $300/1000$	128
N-doped Graphene	CVD	$10\,400 \text{ mA h g}^{-1}$ $200/2.3$	100 cycles $300/1000$	128
Hierarchical C-N architecture	Calcination	$\sim 3000 \text{ mA h g}^{-1}$ $100/2.0$	160 cycles $200/600$	114
S, N-doped graphene oxide	Hummer's method and ultrasonication	$\sim 11\,500 \text{ mA h g}^{-1}$ $100/2.3$	38 cycles $100/1000$	129
Co SA anchored N-doped carbon	Solution method and annealing	$\sim 20\,000 \text{ mA h g}^{-1}$ $200/2.0$	260 cycles $400/1000$	144
CNT-polymer composite	Electrospinning	4800 mA h g^{-1} $0.24 (\text{mA cm}^{-2})/2.0$	22 cycles $0.24 (\text{mA cm}^{-2})/420$	153
Graphene@g-C ₃ N ₄ composite	Hydrothermal Method	$17\,300 \text{ mA h g}^{-1}$ $0.2 (\text{mA cm}^{-2})/2.6$	105 cycles $0.2 (\text{mA cm}^{-2})/1000$	151

Abbreviations: CNT, Carbon nanotube; CVD, chemical vapor deposition.

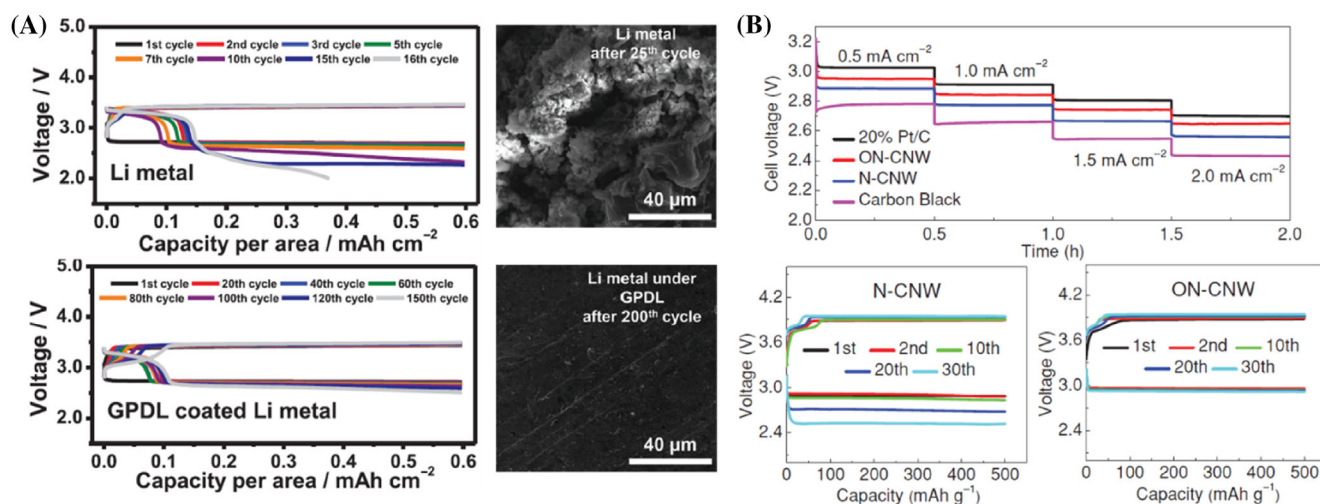


FIGURE 9 (A) Cyclic results for Li–O₂ cells for Li metal and GPD-coated Li metal and SEM images of these cycled electrodes.⁸⁹ Reproduced with permission, 2017, Wiley-VCH. (B) Discharge profiles at various current densities and cyclic performances of hybrid Li–O₂ cells with N-CNw and ON-CNw as the ORR catalyst.¹⁵⁹ Reproduced with permission, Copyright 2014, Wiley-VCH

than that of the cell with Pt/C. Furthermore, this discrepancy decreases when current densities increase, indicating that ON-CNw has excellent catalytic activity in fast electrochemical reactions. The cyclic performances of N-CNw and ON-CNw were also compared. The round-trip overpotential of N-CNw increased from 1.00 to 1.43 V at the first 30 cycles, while that of ON-CNw increased slightly from 0.92 to 1.02 V, revealing the robust cyclic stability of ON-CNw.

4 | CONCLUSION AND PERSPECTIVES

In the review, we discussed the potential of carbonaceous materials for the metal anode protection and host and cathode catalysts of LABs. As the base material for the LAB electrode, methods to synthesize the carbonaceous materials, from graphene to even soft carbons with non-graphitizing properties are introduced. With the intense research on their fabrication and extreme abundance of the element, carbonaceous materials are represented as one of the most cost-effective materials, which is indispensable for the commercialization of the LAB. Furthermore, the intrinsic electric conductivity and light weight lead carbonaceous materials to the most promising candidate for future LAB electrodes. However, the low reactivity and instability for the reaction radicals due to spontaneous defects of carbon were the main bottlenecks for the fabrication of practical LABs with carbonaceous materials. As an answer to those obstacles, the modification strategies for the carbonaceous materials are presented. With the morphology control, the cathode benefits from the expanded surface area, generating

an additional energy capacity, while extra space/channel formation leads to suppression of dendrite and promotion of Li ions for the anode. From the functionalization of carbonaceous materials, the OER/ORR properties of the cathode is boosted by the increase of reaction sites and enhanced charge transfer. Finally, the metal-free composite of the carbonaceous materials even presents the mechanical strength to the electrode, which leads to strengthened cycle stability.

Unfortunately, various approaches to achieve both high cyclic performance and electrode reactivity toward charge–discharge reaction were mostly not successful, suffering from the trade-off between the stability and activity of the carbonaceous materials. As the active sites introduced in the carbon structure also becomes the site for carbon electrode decomposition, further strategies for selective suppression toward decomposition reaction is required. In addition, the modification of the carbonaceous material also deteriorates the electric conductivity which leads to the side reaction. Therefore, there should be more approach toward the optimal degree of the modification, such as surface oxygen groups, dopant introduction or defect generation.

Hopefully, several approaches to the fully carbon-based LABs at the level of practical application have been published lately. As shown in Figure 10A, the rationally designed LAB composed of porous graphene electrodes showed comparable volumetric/gravimetric capacity to commercial batteries.¹⁶⁰ Moreover, with the flexible nature of the carbonaceous materials, the possibility of application to a foldable battery was also suggested in Figure 10B.¹⁶¹ With the rise of the wearable device, the uniqueness of the flexible carbon electrodes may

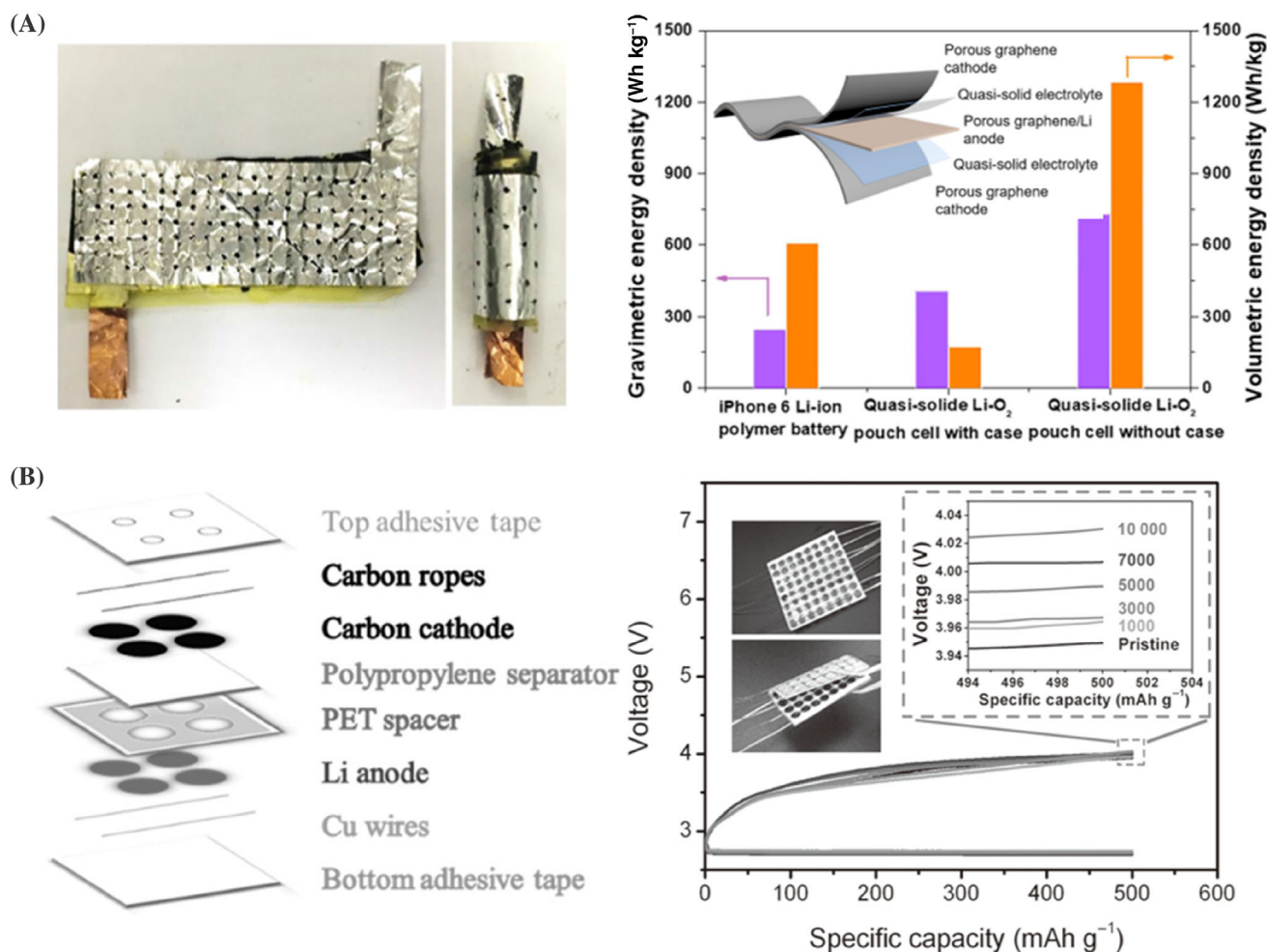


FIGURE 10 (A) Structure and electrochemical properties of the graphene-based pouch cell.¹⁶⁰ Reproduced with permission, Copyright 2018, Springer Nature. (B) The layout of the layers in the battery structure and charge–discharge curves after bended thousands of times.¹⁶¹ Reproduced with permission, Copyright 2016, Wiley-VCH

accelerate the actual application to commercialized batteries. Considering that the fabricated cells for Figure 9 are composed of carbonaceous electrodes without any modifications, if the LAB with optimal modifications are configured, the practical application of fully carbonaceous LAB can be approached one step further.

Although the performance of these fully carbon-based LABs without any modification can reach those of currently commercialized batteries on a laboratory level, further development is imperative for the practical and industrial application. Representatively, the demand for high-performance and long-term stability of full batteries has grown rapidly owing to the rise of diverse electronic industries, electric vehicle, and energy storage system. To fulfill these requirements, the following points should be considered in the future works.

1. The suitable synthesis methods that can precisely control the crystallinity, defect, porous structure,

morphology, surface chemistry, and composite composition of carbonaceous materials should be developed. In addition, the compositional modification, such as doping engineering, single atom catalyst (SAC) decoration, and the formation of composite can further improve the electrocatalytical performances for LAB. The high quality and scalable synthesis of the homogeneous carbon materials need to be guaranteed.

2. For the rational design of the carbonaceous materials, the correlation between structure and property, and the energy storage mechanism of electrodes for LABs should be investigated. Furthermore, the theoretical and experimental approaches toward carbonaceous materials used as active materials and catalysts for LABs have to be carried out using the in-situ/operando spectroscopic analyses and computational calculations.
3. It is needed to optimize the formulation of electrolyte, current collector and binder suitable for the properly

designated carbonaceous electrodes. The development of carbonaceous electrodes with high electrical conductivity enables the freestanding electrodes without the current collector or conducting agent to enhance higher energy density of electrodes in LABs.

4. For the commercialization in LAB, the practical manufacturing factors, such as low production cost and large scalable fabrication with high quality of nanostructured carbons, as well as the cell design and engineering should be cultivated. Moreover, a reliable evaluation system for LAB performances should be constructed, covering the level of full-cell engineering.

Therefore, the persistent research interest and continued breakthroughs including the view of real applications are essential to develop revolutionary carbon-based electrodes for the advanced LAB system, which can significantly enhance the quality of everyday life.

ACKNOWLEDGMENTS

J. Lee and T. H. Lee contributed equally to this work. J. Lee and H. S. Park acknowledge financial support from the National Research Foundation of Korea (NRF) grant funded by the Korea government (MSIT) (NRF-2020M2D8A2070866), Republic of Korea and Korea Initiative for fostering University of Research and Innovation Program of the National Research Foundation (NRF) funded by the Korean government (MSIT) (No. 2020M3H1A1077095). T. H. Lee and H. W. Jang acknowledge financial support from the Basic Science Research Program funded by the Ministry of Science, ICT & Future Planning (2021R1A2B5B03001851) and the National Research Foundation of Korea (NRF) funded by the Ministry of Science and ICT (2020M2D8A206983011).

CONFLICT OF INTEREST

The authors declare no conflict of interest.

ORCID

Jeongyeon Lee  <https://orcid.org/0000-0002-0905-4510>

Ho Won Jang  <https://orcid.org/0000-0002-6952-7359>

Ho Seok Park  <https://orcid.org/0000-0002-4424-4037>

REFERENCES

1. Arunachalam VS, Fleischer EL. The global energy landscape and materials innovation. *MRS Bull.* 2011;33(4):264-288.
2. Dresselhaus MS, Thomas IL. Alternative energy technologies. *Nature.* 2001;414(6861):332-337.
3. Stern PC, Sovacool BK, Dietz T. Towards a science of climate and energy choices. *Nat Clim Change.* 2016;6(6):547-555.
4. Yang Z, Zhang J, Kintner-Meyer MC, et al. Electrochemical energy storage for green grid. *Chem Rev.* 2011;111(5):3577-3613.
5. Dai L, Xue Y, Qu L, Choi HJ, Baek JB. Metal-free catalysts for oxygen reduction reaction. *Chem Rev.* 2015;115(11):4823-4892.
6. Liu X, Dai L. Carbon-based metal-free catalysts. *Nat Rev Mater.* 2016;1:16064.
7. Tarascon JM, Armand M. Issues and challenges facing rechargeable lithium batteries. *Nature.* 2001;414(6861):359-367.
8. Winter M, Brodd RJ. What are batteries, fuel cells, and supercapacitors? *Chem Rev.* 2004;104(10):4245-4269.
9. Dou Q, Wu N, Yuan H, et al. Emerging trends in anion storage materials for the capacitive and hybrid energy storage and beyond. *Chem Soc Rev.* 2021;50(12):6734-6789.
10. Gund GS, Park JH, Harpalsinh R, et al. MXene/polymer hybrid materials for flexible AC-filtering electrochemical capacitors. *Joule.* 2019;3(1):164-176.
11. Nakhanev P, Yu X, Park SK, et al. Revealing molecular-level surface redox sites of controllably oxidized black phosphorus nanosheets. *Nat Mater.* 2019;18(2):156-162.
12. Yeon JS, Ko YH, Park TH, Park H, Kim J, Park HS. Multi-dimensional hybrid architecture encapsulating cobalt oxide nanoparticles into carbon nanotube branched nitrogen-doped reduced graphene oxide networks for lithium-sulfur batteries. *Energy Environ Mater.* 2021;0:1-10. <https://doi.org/10.1002/eem2.12187>
13. Long J, Hou Z, Shu C, et al. Free-standing three-dimensional CuCo₂S₄ nanosheet array with high catalytic activity as an efficient oxygen electrode for lithium-oxygen batteries. *ACS Appl Mater Interfaces.* 2019;11(4):3834-3842.
14. Wang L, Pan J, Zhang Y, Cheng X, Liu L, Peng H. A Li-air battery with ultralong cycle life in ambient air. *Adv Mater.* 2018;30(3):1704378.
15. Xu S-M, Zhu Q-C, Long J, et al. Low-overpotential Li-O₂ batteries based on TFSI intercalated Co-Ti layered double oxides. *Adv Funct Mater.* 2016;26(9):1365-1374.
16. Paul R, Zhu L, Chen H, Qu J, Dai L. Recent advances in carbon-based metal-free electrocatalysts. *Adv Mater.* 2019;31(31):e1806403.
17. Hu C, Dai L. Carbon-based metal-free catalysts for electrocatalysis beyond the ORR. *Angew Chem Int Ed.* 2016;55(39):11736-11758.
18. Zhang L, Lin CY, Zhang D, et al. Guiding principles for designing highly efficient metal-free carbon catalysts. *Adv Mater.* 2019;31(13):e1805252.
19. Lee J-S, Tai Kim S, Cao R, et al. Metal-air batteries with high energy density: Li-air versus Zn-air. *Adv Energy Mater.* 2011;1(1):34-50.
20. Cheon JY, Kim K, Sa YJ, et al. Graphitic nanoshell/nanoporous carbon nanohybrids as highly efficient and stable bifunctional oxygen electrocatalysts for rechargeable aqueous Na-air batteries. *Adv Energy Mater.* 2016;6(7):1501794.
21. Yin W-W, Shadike Z, Yang Y, et al. A long-life Na-air battery based on a soluble NaI catalyst. *Chem Commun.* 2015;51(12):2324-2327.
22. Davari E, Ivey DG. Bifunctional electrocatalysts for Zn-air batteries. *Sustainable Energy Fuels.* 2018;2(1):39-67.
23. Nestoridi M, Pletcher D, Wood RJK, et al. The study of aluminium anodes for high power density Al/air batteries with brine electrolytes. *J Power Sources.* 2008;178(1):445-455.

24. Zhang Z, Zuo C, Liu Z, Yu Y, Zuo Y, Song Y. All-solid-state Al-air batteries with polymer alkaline gel electrolyte. *J Power Sources*. 2014;251:470-475.
25. Hang BT, Hayashi H, Yoon S-H, Okada S, Yamaki JI. Fe₂O₃-filled carbon nanotubes as a negative electrode for an Fe-air battery. *J Power Sources*. 2008;178(1):393-401.
26. Li W, Li C, Zhou C, Ma H, Chen J. Metallic magnesium nano/mesoscale structures: their shape-controlled preparation and mg/air battery applications. *Angew Chem Int Ed*. 2006;45(36):6009-6012.
27. Cheng H, Mao YJ, Xie J, Lu Y, Zhao X. Dendrite-free fluorinated graphene/lithium anodes enabling in situ LiF formation for high-performance lithium-oxygen cells. *ACS Appl Mater Interfaces*. 2019;11(43):39737-39745.
28. Ding Y, Li Y, Wu M, Zhao H, Li Q, Wu ZS. Recent advances and future perspectives of two-dimensional materials for rechargeable Li-O₂ batteries. *Energy Storage Mater*. 2020;31:470-491.
29. Zhao CZ, Zhang XQ, Cheng XB, et al. An anion-immobilized composite electrolyte for dendrite-free lithium metal anodes. *Proc Natl Acad Sci U S A*. 2017;114(42):11069-11074.
30. Guo Z, Li J, Xia Y, et al. A flexible polymer-based Li-air battery using a reduced graphene oxide/Li composite anode. *J Mater Chem A*. 2018;6(14):6022-6032.
31. Wang A, Tang S, Kong D, et al. Bending-tolerant anodes for lithium-metal batteries. *Adv Mater*. 2018;30(1):1703891.
32. Liu T, Vivek JP, Zhao EW, Lei J, Garcia-Araez N, Grey CP. Current challenges and routes forward for nonaqueous lithium-air batteries. *Chem Rev*. 2020;120(14):6558-6625.
33. Zhang X, Cheng X, Zhang Q. Nanostructured energy materials for electrochemical energy conversion and storage: a review. *J Energy Chem*. 2016;25(6):967-984.
34. Zhao Z, Li M, Zhang L, Dai L, Xia Z. Design principles for heteroatom-doped carbon nanomaterials as highly efficient catalysts for fuel cells and metal-air batteries. *Adv Mater*. 2015;27(43):6834-6840.
35. Zhu B, Liang Z, Xia D, Zou R. Metal-organic frameworks and their derivatives for metal-air batteries. *Energy Storage Mater*. 2019;23:757-771.
36. Li Y, Xu Y, Yang W, Shen W, Xue H, Pang H. MOF-derived metal oxide composites for advanced electrochemical energy storage. *Small*. 2018;14(25):e1704435.
37. Oh SH, Nazar LF. Oxide catalysts for rechargeable high-capacity Li-O₂ batteries. *Adv Energy Mater*. 2012;2(7):903-910.
38. Park HW, Lee DU, Zamani P, Seo MH, Nazar LF, Chen Z. Electrospun porous nanorod perovskite oxide/nitrogen-doped graphene composite as a bi-functional catalyst for metal air batteries. *Nano Energy*. 2014;10:192-200.
39. Liu D, Dai L, Lin X, et al. Chemical approaches to carbon-based metal-free catalysts. *Adv Mater*. 2019;31(13):e1804863.
40. Gong KP, Du F, Xia ZH, Durstock M, Dai L. Nitrogen-doped carbon nanotube arrays with high electrocatalytic activity for oxygen reduction. *Science*. 2009;323(5915):760-764.
41. Zhao Y, Nakamura R, Kamiya K, Nakanishi S, Hashimoto K. Nitrogen-doped carbon nanomaterials as non-metal electrocatalysts for water oxidation. *Nat Commun*. 2013;4:2390.
42. Kim J, Choi MS, Shin KH, et al. Rational design of carbon nanomaterials for electrochemical sodium storage and capture. *Adv Mater*. 2019;31(34):e1803444.
43. Geim AK. Graphene: status and prospects. *Science*. 2009;324(5934):1530-1534.
44. Kumar R, Joanni E, Singh RK, Singh DP, Moshkalev SA. Recent advances in the synthesis and modification of carbon-based 2D materials for application in energy conversion and storage. *Prog Energy Combust Sci*. 2018;67:115-157.
45. Rao R, Pint CL, Islam AE, et al. Carbon nanotubes and related nanomaterials: critical advances and challenges for synthesis toward mainstream commercial applications. *ACS Nano*. 2018;12(12):11756-11784.
46. Park SK, Lee H, Choi MS, Suh DH, Nakhanivej P, Park HS. Straightforward and controllable synthesis of heteroatom-doped carbon dots and nanoporous carbons for surface-confined energy and chemical storage. *Energy Storage Mater*. 2018;12:331-340.
47. Destyorini F, Irmawati Y, Hardiansyah A, et al. Formation of nanostructured graphitic carbon from coconut waste via low-temperature catalytic graphitisation. *Eng Sci Technol Int J*. 2021;24(2):514-523.
48. Dhakate SR, Mathur RB, Bahl OP. Catalytic effect of iron oxide on carbon/carbon composites during graphitization. *Carbon*. 1997;35(12):1753-1756.
49. Iwazaki T, Semba T, Konishi S, et al. Catalytic excavation and graphitization of activated carbon by cobalt nanoparticles. *Chem Lett*. 2008;37(12):1194-1195.
50. Wang KL, Cao YH, Wang XM, et al. Nickel catalytic graphitized porous carbon as electrode material for high performance supercapacitors. *Energy*. 2016;101:9-15.
51. Thompson E, Danks AE, Bourgeois L, Schnepf Z. Iron-catalyzed graphitization of biomass. *Green Chem*. 2015;17(1):551-556.
52. Lee C, Wei XD, Kysar JW, Hone J. Measurement of the elastic properties and intrinsic strength of monolayer graphene. *Science*. 2008;321(5887):385-388.
53. Cooper AJ, Wilson NR, Kinloch IA, Dryfe RAW. Single stage electrochemical exfoliation method for the production of few-layer graphene via intercalation of tetraalkylammonium cations. *Carbon*. 2014;66:340-350.
54. Ciesielski A, Samori P. Graphene via sonication assisted liquid-phase exfoliation. *Chem Soc Rev*. 2014;43(1):381-398.
55. Novoselov KS, Geim AK, Morozov SV, et al. Electric field effect in atomically thin carbon films. *Science*. 2004;306(5696):666-669.
56. Huang Y, Sutter E, Shi NN, et al. Reliable exfoliation of large-area high-quality flakes of graphene and other two-dimensional materials. *ACS Nano*. 2015;9(11):10612-10620.
57. Su CY, Lu AY, Xu YP, Chen FR, Khlobystov AN, Li LJ. High-quality thin graphene films from fast electrochemical exfoliation. *ACS Nano*. 2011;5(3):2332-2339.
58. Sampath S, Basuray AN, Hartlieb KJ, Aytun T, Stupp SI, Stoddart JF. Direct exfoliation of graphite to graphene in aqueous media with diazaperopyrenium dications. *Adv Mater*. 2013;25(19):2740-2745.
59. Lee Y, Bae S, Jang H, et al. Wafer-scale synthesis and transfer of graphene films. *Nano Lett*. 2010;10(2):490-493.
60. Wang X, Chen W, Zhang L, et al. Uncoordinated amine groups of metal-organic frameworks to anchor single Ru sites as chemoselective catalysts toward the hydrogenation of quinoline. *J Am Chem Soc*. 2017;139(28):9419-9422.

61. Liu M, Lee J, Yang TC, et al. Synergies of Fe single atoms and clusters on N-doped carbon electrocatalyst for pH-universal oxygen reduction. *Small Methods*. 2021;5(5):2001165.
62. Liu F, Wang C, Sui X, et al. Synthesis of graphene materials by electrochemical exfoliation: recent progress and future potential. *Carbon Energy*. 2019;1(2):173-199.
63. Tan CL, Cao XH, Wu XJ, et al. Recent advances in ultrathin two-dimensional nanomaterials. *Chem Rev*. 2017;117(9):6225-6331.
64. Yang W, Zhang X, Xie Y. Advances and challenges in chemistry of two-dimensional nanosheets. *Nano Today*. 2016;11(6):793-816.
65. Edwards RS, Coleman KS. Graphene film growth on polycrystalline metals. *Acc Chem Res*. 2013;46(1):23-30.
66. Lee HC, Liu W-W, Chai S-P, et al. Synthesis of single-layer graphene: a review of recent development. *Procedia Chem*. 2016;19:916-921.
67. Strupinski W, Grodecki K, Wyszomolek A, et al. Graphene epitaxy by chemical vapor deposition on SiC. *Nano Lett*. 2011;11(4):1786-1791.
68. Yu QK, Lian J, Siriponglert S, Li H, Chen YP, Pei SS. Graphene segregated on Ni surfaces and transferred to insulators. *Appl Phys Lett*. 2008;93(11):113103.
69. Benziger MR, Talapaneni SN, Joseph S, et al. Recent advances in functionalized micro and mesoporous carbon materials: synthesis and applications. *Chem Soc Rev*. 2018;47(8):2680-2721.
70. Titirici MM, Thomas A, Antonietti M. Replication and coating of silica templates by hydrothermal carbonization. *Adv Funct Mater*. 2007;17(6):1010-1018.
71. Schuster J, He G, Mandlmeier B, et al. Spherical ordered mesoporous carbon nanoparticles with high porosity for lithium-sulfur batteries. *Angew Chem Int Ed*. 2012;51(15):3591-3595.
72. Li J-C, Hou P-X, Zhao S-Y, et al. A 3D bi-functional porous N-doped carbon microtube sponge electrocatalyst for oxygen reduction and oxygen evolution reactions. *Energy Environ Sci*. 2016;9(10):3079-3084.
73. Pei Z, Li H, Huang Y, et al. Texturing in situ: N,S-enriched hierarchically porous carbon as a highly active reversible oxygen electrocatalyst. *Energy Environ Sci*. 2017;10(3):742-749.
74. Lin Z, Waller GH, Liu Y, Liu M, Wong CP. 3D Nitrogen-doped graphene prepared by pyrolysis of graphene oxide with polypyrrole for electrocatalysis of oxygen reduction reaction. *Nano Energy*. 2013;2(2):241-248.
75. Liu R, Wu D, Feng X, Mullen K. Nitrogen-doped ordered mesoporous graphitic arrays with high electrocatalytic activity for oxygen reduction. *Angew Chem Int Ed*. 2010;122(14):2619-2623.
76. Zhang LL, Zhao X, Ji H, et al. Nitrogen doping of graphene and its effect on quantum capacitance, and a new insight on the enhanced capacitance of N-doped carbon. *Energy Environ Sci*. 2012;5(11):9618-9625.
77. Zhao L, Zhang Y, Huang LB, et al. Cascade anchoring strategy for general mass production of high-loading single-atomic metal-nitrogen catalysts. *Nat Commun*. 2019;10(1):1278.
78. Zhu C, Shi Q, Xu BZ, et al. Hierarchically porous M-N-C (M = Co and Fe) single-atom electrocatalysts with robust MN_x active moieties enable enhanced ORR performance. *Adv Energy Mater*. 2018;8(29):1801956.
79. Gao MR, Cao X, Gao Q, et al. Nitrogen-doped graphene supported CoSe₂ nanobelt composite catalyst for efficient water oxidation. *ACS Nano*. 2014;8(4):3970-3978.
80. Hu C, Xiao Y, Zhao Y, et al. Highly nitrogen-doped carbon capsules: scalable preparation and high-performance applications in fuel cells and lithium ion batteries. *Nanoscale*. 2013;5(7):2726-2733.
81. Barton TJ, Bull LM, Klemperer WG, et al. Tailored porous materials. *Chem Mater*. 1999;11(10):2633-2656.
82. Guo S, Peng J, Li W, et al. Effects of CO₂ activation on porous structures of coconut shell-based activated carbons. *Appl Surf Sci*. 2009;255(20):8443-8449.
83. Yoon S-H, Lim S, Song Y, et al. KOH activation of carbon nanofibers. *Carbon*. 2004;42(8-9):1723-1729.
84. Lee J, Kim J, Hyeon T. A facile synthesis of bimodal mesoporous silica and its replication for bimodal mesoporous carbon. *Chem Commun*. 2003;(10):1138-1139.
85. Lee J, Sohn K, Hyeon T. Fabrication of novel mesocellular carbon foams with uniform ultralarge mesopores. *J Am Chem Soc*. 2001;123(21):5146-5147.
86. Zhang R, Chen XR, Chen X, et al. Lithiophilic sites in doped graphene guide uniform lithium nucleation for dendrite-free lithium metal anodes. *Angew Chem Int Ed*. 2017;56(27):7764-7768.
87. Peled E, Menkin S. Review—SEI: past, present and future. *J Electrochem Soc*. 2017;164(7):A1703-A1719.
88. Lin D, Liu Y, Liang Z, et al. Layered reduced graphene oxide with nanoscale interlayer gaps as a stable host for lithium metal anodes. *Nat Nanotechnol*. 2016;11(7):626-632.
89. Kwak WJ, Park SJ, Jung HG, Sun YK. Optimized concentration of redox mediator and surface protection of Li metal for maintenance of high energy efficiency in Li-O₂ batteries. *Adv Energy Mater*. 2018;8(9):1702258.
90. Ma Y, Wei L, Gu Y, et al. High-performance Li-O₂ batteries based on all-graphene backbone. *Adv Funct Mater*. 2020;30(51):2007218.
91. Bai W-L, Zhang Z, Chen X, et al. Boosting the electrochemical performance of Li-O₂ batteries with DPPH redox mediator and graphene-luteolin-protected lithium anode. *Energy Storage Mater*. 2020;31:373-381.
92. Bobnar J, Lozinšek M, Kapun G, et al. Fluorinated reduced graphene oxide as a protective layer on the metallic lithium for application in the high energy batteries. *Sci Rep*. 2018;8(1):5819.
93. Vizintin A, Patel MUM, Genorio B, Dominko R. Effective separation of lithium anode and sulfur cathode in lithium-sulfur batteries. *ChemElectroChem*. 2014;1(6):1040-1045.
94. Vizintin A, Lozinšek M, Chellappan RK, et al. Fluorinated reduced graphene oxide as an interlayer in Li-S batteries. *Chem Mater*. 2015;27(20):7070-7081.
95. Chen X, Chen X-R, Hou T-Z, et al. Lithiophilicity chemistry of heteroatom-doped carbon to guide uniform lithium nucleation in lithium metal anodes. *Sci Adv*. 2019;5(2):eaau7728.
96. Li S, Liu Q, Zhou J, et al. Hierarchical Co₃O₄ nanofiber-carbon sheet skeleton with superior Na/Li-philic property enabling highly stable alkali metal batteries. *Adv Funct Mater*. 2019;29(19):1808847.
97. Zheng GY, Lee SW, Liang Z, et al. Interconnected hollow carbon nanospheres for stable lithium metal anodes. *Nat Nanotechnol*. 2014;9(8):618-623.

98. Liu YP, Zhen YZ, Li TR, et al. High-capacity, dendrite-free, and ultrahigh-rate lithium-metal anodes based on monodisperse N-doped hollow carbon nanospheres. *Small*. 2020;16(44):2004770.
99. Chen M, Zheng JH, Sheng OW, et al. Sulfur–nitrogen co-doped porous carbon nanosheets to control lithium growth for a stable lithium metal anode. *J Mater Chem A*. 2019;7(31):18267–18274.
100. An YL, Tian Y, Li Y, et al. Heteroatom-doped 3D porous carbon architectures for highly stable aqueous zinc metal batteries and non-aqueous lithium metal batteries. *Chem Eng J*. 2020;400:125843.
101. Ren F, Peng Z, Wang M, et al. Over-potential induced Li/Na filtrated depositions using stacked graphene coating on copper scaffold. *Energy Storage Mater*. 2019;16:364–373.
102. Liu S, Wang A, Li Q, et al. Crumpled graphene balls stabilized dendrite-free lithium metal anodes. *Joule*. 2018;2(1):184–193.
103. Moorthy B, Kim J-H, Lee H-W, Kim DK. Vertically aligned carbon nanotubular structure for guiding uniform lithium deposition via capillary pressure as stable metallic lithium anodes. *Energy Storage Mater*. 2020;24:602–609.
104. Sun Z, Jin S, Jin H, et al. Robust expandable carbon nanotube scaffold for ultrahigh-capacity lithium-metal anodes. *Adv Mater*. 2018;30(32):e1800884.
105. Zhang M, Lu R, Yuan H, et al. Nanowire array-coated flexible substrate to accommodate lithium plating for stable lithium-metal anodes and flexible lithium-organic batteries. *ACS Appl Mater Interfaces*. 2019;11(23):20873–20880.
106. Zuo TT, Wu XW, Yang CP, et al. Graphitized carbon fibers as multifunctional 3D current collectors for high areal capacity Li anodes. *Adv Mater*. 2017;29(29):1700389.
107. Shi P, Li T, Zhang R, et al. Lithiophilic LiC₆ layers on carbon hosts enabling stable Li metal anode in working batteries. *Adv Mater*. 2019;31(8):e1807131.
108. Huang G, Han J, Zhang F, et al. Lithiophilic 3D nanoporous nitrogen-doped graphene for dendrite-free and ultrahigh-rate lithium-metal anodes. *Adv Mater*. 2019;31(2):e1805334.
109. Song H, Chen X, Zheng G, et al. Dendrite-free composite Li anode assisted by Ag nanoparticles in a wood-derived carbon frame. *ACS Appl Mater Interfaces*. 2019;11(20):18361–18367.
110. Zhang Y, Luo W, Wang C, et al. High-capacity, low-tortuosity, and channel-guided lithium metal anode. *Proc Natl Acad Sci U S A*. 2017;114(14):3584–3589.
111. Niu C, Pan H, Xu W, et al. Self-smoothing anode for achieving high-energy lithium metal batteries under realistic conditions. *Nat Nanotechnol*. 2019;14(6):594–601.
112. Sun B, Wang B, Su D, Xiao L, Ahn H, Wang G. Graphene nanosheets as cathode catalysts for lithium-air batteries with an enhanced electrochemical performance. *Carbon*. 2012;50(2):727–733.
113. Xiao J, Mei D, Li X, et al. Hierarchically porous graphene as a lithium–air battery electrode. *Nano Lett*. 2011;11(11):5071–5078.
114. Zhang Z, Bao J, He C, Chen Y, Wei J, Zhou Z. Hierarchical carbon–nitrogen architectures with both mesopores and macrochannels as excellent cathodes for rechargeable Li–O₂ batteries. *Adv Funct Mater*. 2014;24(43):6826–6833.
115. Lim H-D, Park K-Y, Song H, et al. Enhanced power and rechargeability of a Li–O₂ battery based on a hierarchical-fibril CNT electrode. *Adv Mater*. 2013;25(9):1348–1352.
116. Shu C, Li B, Zhang B, Su D. Hierarchical nitrogen-doped graphene/carbon nanotube composite cathode for lithium–oxygen batteries. *ChemSusChem*. 2015;8(23):3973–3976.
117. Qian Z, Guo R, Ma Y, et al. Se-doped carbon as highly stable cathode material for high energy nonaqueous Li–O₂ batteries. *Chem Eng Sci*. 2020;214:115413.
118. Wu A, Wei G, Yang F, et al. Nitrogen and iodine dual-doped 3D porous graphene as a bi-functional cathode catalyst for Li–O₂ batteries. *Electrochim Acta*. 2019;318:354–361.
119. Zhou W, Zhang H, Nie H, Ma Y, Zhang Y, Zhang H. Hierarchical micron-sized mesoporous/macroporous graphene with well-tuned surface oxygen chemistry for high capacity and cycling stability Li–O₂ battery. *ACS Appl Mater Interfaces*. 2015;7(5):3389–3397.
120. Lv W, Tang D-M, He Y-B, et al. Low-temperature exfoliated graphenes: vacuum-promoted exfoliation and electrochemical energy storage. *ACS Nano*. 2009;3(11):3730–3736.
121. Zhong X, Papandrea B, Xu Y, et al. Three-dimensional graphene membrane cathode for high energy density rechargeable lithium-air batteries in ambient conditions. *Nano Res*. 2017;10(2):472–482.
122. Laoire CO, Mukerjee S, Plichta EJ, Hendrickson MA, Abraham KM. Rechargeable lithium/TEGDME–LiPF₆/O₂ battery. *J Electrochem Soc*. 2011;158(3):A302–A308.
123. Duan J, Chen S, Jaroniec M, Qiao SZ. Heteroatom-doped graphene-based materials for energy-relevant electrocatalytic processes. *ACS Catal*. 2015;5(9):5207–5234.
124. Wang X, Sun G, Routh P, Kim DH, Huang W, Chen P. Heteroatom-doped graphene materials: syntheses, properties and applications. *Chem Soc Rev*. 2014;43(20):7067–7098.
125. Sakaushi K, Fellingner T-P, Antonietti M. Bifunctional metal-free catalysis of mesoporous noble carbons for oxygen reduction and evolution reactions. *ChemSusChem*. 2015;8(7):1156–1160.
126. Yun K-H, Hwang Y, Chung Y-C. Effective catalytic media using graphitic nitrogen-doped site in graphene for a non-aqueous Li–O₂ battery: a density functional theory study. *J Power Sources*. 2015;277:222–227.
127. Jing Y, Zhou Z. Computational insights into oxygen reduction reaction and initial Li₂O₂ nucleation on pristine and N-doped graphene in Li–O₂ batteries. *ACS Catal*. 2015;5(7):4309–4317.
128. Han J, Guo X, Ito Y, et al. Effect of chemical doping on cathodic performance of bicontinuous nanoporous graphene for Li–O₂ batteries. *Adv Energy Mater*. 2016;6(3):1501870.
129. Kim J-H, Kannan AG, Woo H-S, et al. A bi-functional metal-free catalyst composed of dual-doped graphene and mesoporous carbon for rechargeable lithium–oxygen batteries. *J Mater Chem A*. 2015;3(36):18456–18465.
130. Trahan MJ, Gunasekara I, Mukerjee S, Plichta EJ, Hendrickson MA, Abraham KM. Solvent-coupled catalysis of the oxygen electrode reactions in lithium-air batteries. *J Electrochem Soc*. 2014;161(10):A1706–A1715.
131. Zimmerman MT, Bayse CA, Ramoutar RR, Brumaghi JL. Sulfur and selenium antioxidants: challenging radical scavenging mechanisms and developing structure–activity relationships based on metal binding. *J Inorg Biochem*. 2015;145:30–40.
132. Li F, Li T, Sun C, Xia J, Jiao Y, Xu H. Selenium-doped carbon quantum dots for free-radical scavenging. *Angew Chem Int Ed*. 2017;56(33):9910–9914.
133. Yoo E, Zhou H. Li–air rechargeable battery based on metal-free graphene nanosheet catalysts. *ACS Nano*. 2011;5(4):3020–3026.

134. Bae Y, Yun YS, Lim H-D, et al. Tuning the carbon crystallinity for highly stable Li–O₂ batteries. *Chem Mater*. 2016;28(22):8160–8169.
135. Li S, Wang M, Yao Y, Zhao T, Yang L, Wu F. Effect of the activation process on the microstructure and electrochemical properties of N-doped carbon cathodes in Li–O₂ batteries. *ACS Appl Mater Interfaces*. 2019;11(38):34997–35004.
136. Shui J, Du F, Xue C, Li Q, Dai L. Vertically aligned N-doped coral-like carbon fiber arrays as efficient air electrodes for high-performance nonaqueous Li–O₂ batteries. *ACS Nano*. 2014;8(3):3015–3022.
137. Meng X, Liao K, Dai J, et al. Ultralong cycle life Li–O₂ battery enabled by a MOF-derived ruthenium–carbon composite catalyst with a durable regenerative surface. *ACS Appl Mater Interfaces*. 2019;11(22):20091–20097.
138. Jiang Z-L, Sun H, Shi W-K, et al. P-doped hive-like carbon derived from pinecone biomass as efficient catalyst for Li–O₂ battery. *ACS Sustain Chem Eng*. 2019;7(16):14161–14169.
139. Hernández-Rentero C, Córdoba R, Moreno N, et al. Low-cost disordered carbons for Li/S batteries: a high-performance carbon with dual porosity derived from cherry pits. *Nano Res*. 2018;11(1):89–100.
140. Ochai-Ejeh FO, Momodu DY, Madito MJ, et al. Nanostructured porous carbons with high rate cycling and floating performance for supercapacitor application. *AIP Adv*. 2018;8(5):055208.
141. Li Y, Li X, Geng D, et al. Carbon black cathodes for lithium oxygen batteries: influence of porosity and heteroatom-doping. *Carbon*. 2013;64:170–177.
142. Pei C, Choi MS, Yu X, Xue H, Xia BY, Park HS. Recent progress in emerging metal and covalent organic frameworks for electrochemical and functional capacitors. *J Mater Chem A*. 2021;9(14):8832–8869.
143. Hu X, Luo G, Zhao Q, et al. Ru single atoms on N-doped carbon by spatial confinement and ionic substitution strategies for high-performance Li–O₂ batteries. *J Am Chem Soc*. 2020;142(39):16776–16786.
144. Wang P, Ren Y, Wang R, et al. Atomically dispersed cobalt catalyst anchored on nitrogen-doped carbon nanosheets for lithium–oxygen batteries. *Nat Commun*. 2020;11(1):1576.
145. Nong J, Xie P, Zhu AS, Rong MZ, Zhang MQ. Highly conductive doped carbon framework as binder-free cathode for hybrid Li–O₂ battery. *Carbon*. 2019;142:177–189.
146. Jo H-G, Ahn H-J. Accelerating the oxygen reduction reaction and oxygen evolution reaction activities of N and P co-doped porous activated carbon for Li–O₂ batteries. *Catalysts*. 2020;10(11):1316.
147. Lee M, Yoo Y, Kwak JH, et al. Effect of surface characteristics of carbon host on electrochemical performance of non-aqueous Li–O₂ batteries. *Chem Eng J*. 2021;412:128549.
148. Wang Z, Li S, Zhang Y, Xu H. Oxocarbon-functionalized graphene as a lithium-ion battery cathode: a first-principles investigation. *Phys Chem Chem Phys*. 2018;20(11):7447–7456.
149. Lim H-D, Lee B, Bae Y, et al. Reaction chemistry in rechargeable Li–O₂ batteries. *Chem Soc Rev*. 2017;46(10):2873–2888.
150. Wong RA, Dutta A, Yang C, et al. Structurally tuning Li₂O₂ by controlling the surface properties of carbon electrodes: implications for Li–O₂ batteries. *Chem Mater*. 2016;28(21):8006–8015.
151. Luo W-B, Chou S-L, Wang J-Z, Zhai YC, Liu HK. A metal-free, free-standing, macroporous graphene@g-C₃N₄ composite air electrode for high-energy lithium oxygen batteries. *Small*. 2015;11(23):2817–2824.
152. Yi J, Liao K, Zhang C, Zhang T, Li F, Zhou H. Facile in situ preparation of graphitic-C₃N₄@carbon paper as an efficient metal-free cathode for nonaqueous Li–O₂ battery. *ACS Appl Mater Interfaces*. 2015;7(20):10823–10827.
153. Lim AC, Kwon HJ, Lee HC, et al. Mechanically reinforced-CNT cathode for Li–O₂ battery with enhanced specific energy via ex situ pore formation. *Chem Eng J*. 2020;385:123841.
154. Tan P, Shyy W, Wei ZH, An L, Zhao TS. A carbon powder-nanotube composite cathode for non-aqueous lithium–air batteries. *Electrochim Acta*. 2014;147:1–8.
155. Niu W, Marcus K, Zhou L, et al. Enhancing electron transfer and electrocatalytic activity on crystalline carbon-conjugated g-C₃N₄. *ACS Catal*. 2018;8(3):1926–1931.
156. Liu Q, Zhang J. Graphene supported Co-g-C₃N₄ as a novel metal–macrocylic electrocatalyst for the oxygen reduction reaction in fuel cells. *Langmuir*. 2013;29(11):3821–3828.
157. Yan SC, Li ZS, Zou ZG. Photodegradation performance of g-C₃N₄ fabricated by directly heating melamine. *Langmuir*. 2009;25(17):10397–10401.
158. Zhang S, Tsuzuki S, Ueno K, Dokko K, Watanabe M. Upper limit of nitrogen content in carbon materials. *Angew Chem Int Ed*. 2015;54(4):1302–1306.
159. Li L, Manthiram A. O- and N-doped carbon nanowires as metal-free catalysts for hybrid Li–air batteries. *Adv Energy Mater*. 2014;4(10):1301795.
160. Huang G, Han J, Yang C, et al. Graphene-based quasi-solid-state lithium–oxygen batteries with high energy efficiency and a long cycling lifetime. *NPG Asia Mater*. 2018;10(11):1037–1045.
161. Liu T, Xu J-J, Liu Q-C, et al. Ultrathin, lightweight, and wearable Li–O₂ battery with high robustness and gravimetric/volumetric energy density. *Small*. 2017;13(6):1602952.

AUTHOR BIOGRAPHIES



Jeongyeon Lee obtained his Ph.D. from the Department of Nanoscience and Technology of Seoul National University in 2019 and then proceeded to study as a postdoctoral fellow in The Hong Kong Polytechnic University (Department of Applied Biology and Chemical Technology) and Sungkyunkwan University (Department of Chemical Engineering) for two and a half years. Dr. Lee is currently working at the Institute of Textiles and Clothing in The Hong Kong Polytechnic University as a research assistant professor. His research interests lie primarily in the fields of energy storage/conversion applications.



Ho Won Jang is a full professor in the Department of Materials Science and Engineering at Seoul National University. He earned his Ph.D. from the Department of Materials Science and Engineering of Pohang University of Science and Technology in 2004. He worked as a research associate at the University of Madison-Wisconsin from 2006 to 2009. Before he joined Seoul National University in 2012, he worked at the Korea Institute of Science and Technology as a senior research scientist. He is a member of the Young Korean Academy of Science and Technology. His research interests include materials synthesis and device fabrication for solar fuel generation, chemical sensing, nonvolatile data storage, neuromorphic computing, plasmonics, ferroelectronics, and metal-insulator transition. He has published more than 450 papers in international refereed journals.



Ho Seok Park is a professor of Chemical Engineering at the Sungkyunkwan University (SKKU), an adjunct professor at the Samsung Advanced Institute for Health Science & Technology (SAIHST), and a director of the research center for 2D Redox Energy Storage (2DRES). He received his Ph.D. from Korea

Advanced Institute of Science & Technology (KAIST) in 2008 and worked as a postdoctoral researcher in the Department of Biological Engineering at the Massachusetts Institute of Technology (MIT) from 2008 to 2010. His current research interests focus on energy and chemical storage materials and devices based on 2D and carbon nanomaterials. He has published >220 peer-reviewed papers in the top journals and being taking associate editor, editorial board member, and guest editor in the SCI(E) journals of “Advanced Functional Materials”, “InfoMat”, “Energy Storage & Saving”, “Batteries & Supercaps”, “Carbon Letters”, and “Macromolecular Research”.

How to cite this article: Lee J, Lee TH, Jang HW, Park HS. Chemical modification of ordered/disordered carbon nanostructures for metal hosts and electrocatalysts of lithium-air batteries. *InfoMat*. 2022;4(1):e12268. doi:10.1002/inf2.12268